Computational Study of CO_2 Activation on Al_2O_3 Single-Atom Catalyst under External Electric Field

Dissertation submitted to

Visvesvaraya National Institute of Technology, Nagpur

in partial fulfilment of the requirements for the award of the degree

Master of Science
in
Physics

by

Prashik Arun Shahare(MS23PHY023)

Under the guidance of

Dr. Poorva Singh

Department of Physics
Visvesvaraya National Institute of Technology
Nagpur 440010 (India)
2024-2025

VISVESVARAYA NATIONAL INSTITUTE OF TECHNOLOGY,
NAGPUR
DEPARTMENT OF PHYSICS

Dissertation approval sheet

Dissertation entitled "**Computational Study of CO_2 Activation on Al_2O_3 Single-Atom Catalyst under External Electric Field**" by **Prashik Arun Shahare)** Enrollment No. **MS23PHY023** ID No. **30758** is approved for the degree of Master of Science in Physics.

_____

(Name:)

Supervisor

_____

(Name:)

External Examiner

_____

(Name:)

Chairman

Department of Physics

Visvesvaraya National Institute of Technology, Nagpur

Declaration

I, Prashik Arun Shahare, hereby declare that this dissertation titled " **Computational Study of CO_2 Activation on Al_2O_3 Single-Atom Catalyst under External Electric Field**" is carried out by me in the Department of Physics of Visvesvaraya National Institute of Technology, Nagpur. The work is original and has not been submitted earlier whole or in part for the award of any degree/diploma at this or any other Institution / University.

Prashik Arun Shahare

Date: - -2025

Certificate

This to certify that the dissertation titled "**Computational Study of CO_2 Activation on Al_2O_3 Single-Atom Catalyst under External Electric Field** is submitted by **Prashik Arun Shahare** in partial fulfillment of the requirements for the award of the degree of **Master of Science in Physics**, VNIT Nagpur. The work is comprehensive, complete and fit for final evaluation.

Dr. Poorva Singh

Assistant Professor

Physics Dept, VNIT, Nagpur

Head, Department of Physics

VNIT, Nagpur

Date: - -2025

VISVESVARAYA NATIONAL INSTITUTE OF TECHNOLOGY NAGPUR

Non-Plagiarism Certificate

Certified that M.Sc. dissertation titled "**Computational Study of CO_2 Activation on Al_2O_3 Single-Atom Catalyst under External Electric Field**" submitted by **Prashik Arun Shahare**, Enrollment No. **MS23PHY023**, ID No. **30758** has been checked for plagiarism using TURNITIN software and overlap is found within prescribed limits. A summary of the report given below;

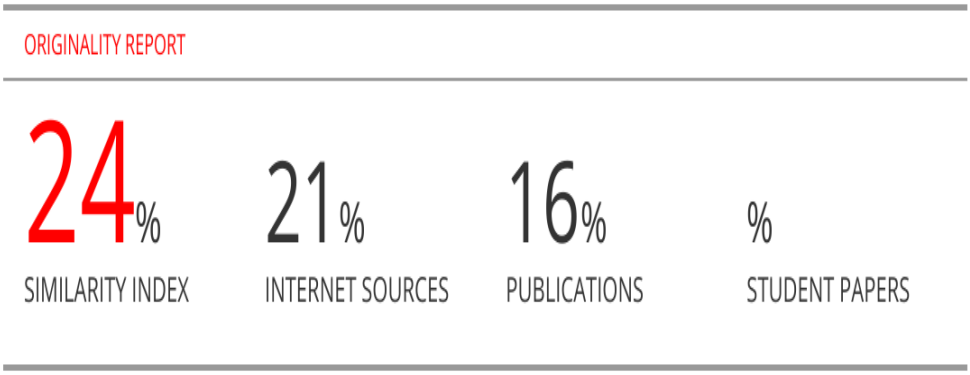

Prashik Arun Shahare
MS23PHY023

Dr. Poorva Singh
Supervisor

ACKNOWLEDGEMENT

I would like to convey my gratitude to my project guide Dr. **Poorva Singh** , Assistant Professor, Department of Physics, Visvesvaraya National Institute of Technology Nagpur, for motivating me and guiding me much in my project work. I will be failing in my duty if I do not acknowledge her with a special thanks. This acknowledgement can not represent the the volcano of feelings that is rumbling to burst out of me through words. I feel highly obliged to have her as my guide. I am highly grateful to her for always been the support system. It's been an honour to work with her.

I am highly thankful to Head of the Department,Department of Physics, VNIT Nagpur, **Dr. Babasaheb R. Sankapal** and all professors for their precious cooperation throughout the session.

I convey my deep gratitude to **Mr. Ajit Singh Jhala**, Ph.D. scholar, who had to bear a heavy load of responsibility and concern in bringing this project to a successful end. He has been a great mentor and without him this project would have been a distant reality.

Prashik Arun Shahare

MS23PHY023

ABSTRACT

This thesis presents a first-principles study of CO_2 activation on the (110) surface of Al_2O_3 decorated with single metal atoms—Co, Cu, and Ag—under the influence of an external electric field. Density Functional Theory (DFT) calculations are performed using the SIESTA (Spanish Initiative for Electronic Simulations with Thousands of Atoms) package. The study investigates how the choice of metal and the application of an electric field affect CO_2 adsorption and dissociation behavior. Charge density difference (CDD) analyses and their corresponding planar averaged profiles along the z-direction are computed to understand charge redistribution at the interface. Additionally, the projected density of states (pDOS) is evaluated to examine the electronic interactions between the adsorbate and the catalytic surface. The results highlight the role of the metal center and external electric field in modulating charge transfer and surface reactivity, offering insight into the rational design of electric field-tunable catalysts for CO_2 conversion.

List of Figures

1.1 Energy profile of the CO_2 activation and dissociation reaction, illustrating the thermodynamic challenge. The reaction pathway from CO_2 to CO + $\frac{1}{2}O_2$ is endothermic, requiring significant activation energy (E_a) to overcome the energy barrier. The enthalpy change (ΔH) reflects the net energy input for the reaction. 4

1.2 Energy-distance relationship for physisorption and chemisorption. Chemisorption (blue) occurs at shorter distance d_{ch} with deeper energy well; physisorption (magenta) occurs at longer distance d_{ph} with a shallower well. 8

1.3 Schematic representation of a single Ag atom deposited on the $(1\bar{1}0)$ surface of an Al_2O_3 + Ag system. (Left) The Ag atom is adsorbed on the surface. (Right) CO_2 molecule interacting with the Ag site on a highly reactive surface, highlighting the potential catalytic activity. . 9

2.1 Flow chart for the scf calculation to solve Kohn-Sham equations. . . . 21

3.1 Side and Top views of the relaxed Al_2O_3-Ag-CO_2 structure visualized using VESTA. 34

3.2 Top and side views of the Al_2O_3-Co-CO_2 relaxed structure. 37

3.3 Al_2O_3-Cu-CO_2 structure visualized using VESTA.. 40

3.4 Binding energies of CO_2 on Al_2O_3 + M surfaces, where M = Co, Cu, and Ag. 51

3.5 Charge density difference (CDD) isosurface 52

3.6 Linear profile of CDD along Z-axis 52
3.7 Charge density difference analysis for Al_2O_3 + Co + CO_2 system . . 52
3.8 Charge density difference (CDD) isosurface 53
3.9 Charge density difference analysis for Al_2O_3 + Cu + CO_2 system . . 53
3.10 Charge density difference (CDD) isosurface 53
3.11 Linear profile of CDD along Z-axis 53
3.12 Charge density difference analysis for Al_2O_3 + Ag + CO_2 system . . 53
3.13 Linear profile of charge density difference (CDD) along Z-axis for Al_2O_3 + Co + CO_2 system under applied electric fields (E = +0.5 V/Å, red curve and E = -0.5 V/Å, blue curve) 54

CONTENTS

Abstract **i**

List of Figures **ii**

Contents **iv**

1 INTRODUCTION **2**

1.1 Introduction 2

1.2 CO_2 Activation and Dissociation: A Thermodynamic Challenge . . . 4

1.3 Physisorption vs Chemisorption of CO_2 on Catalyst Surfaces 6

1.4 Reducible and Irreducible Substrates in Catalysis and Plasma-Driven CO_2 Activation 9

2 CONCEPTS AND COMPUTATIONAL METHODOLOGY **12**

2.1 Approximation Method 12

2.2 The Born-Oppenheimer approximation 13

2.3 Density Functional Theory Approach 14

2.3.1 The Theorems of Hohenberg and Kohn 15

2.3.2 The Kohn-Sham equation 18

2.3.3 The exchange-correlation functional 22

2.3.4 Spin-Orbit Interaction 23

2.4 Solving the equations 24

2.5 Applications of DFT 25

2.5.1 Equilibrium Structure 25
2.5.2 Band Structures and Density of States (DOS) 26
2.6 Computational Package 27
2.6.1 VASP 27
2.6.2 LAMMPS 29
2.6.3 SIESTA 29

3 Electronic Structure and Interaction Analysis of Single Metal Atoms on Al_2O_3 Surface 33

3.1 Structure 33
3.1.1 Al_2O_3-Ag-CO_2 Configuration 33
3.1.2 Al_2O_3-Co-CO_2 Configuration 37
3.1.3 [Al_2O_3-Cu-CO_2 Configuration] 40
3.1.4 INPUT FILE 43
3.2 Results and Discussion 49
3.2.1 Binding Energy Calculation 49
3.3 Charge Density Difference Analysis 50
3.3.1 Al_2O_3 + Co + CO_2 System 52
3.3.2 Al_2O_3 + Cu + CO_2 System 53
3.3.3 Al_2O_3 + Ag + CO_2 System 53
3.3.4 Charge Density Difference Under Electric Field 54

4 SUMMARY AND CONCLUSION 57

References 59

INTRODUCTION

Chapter 1

INTRODUCTION

1.1 Introduction

Over the past few decades, the growing global energy demand has significantly elevated air pollution levels. One of the main concerns is the rise in greenhouse gases, especially carbon dioxide (CO_2), primarily due to the combustion of fossil fuels, which has led to serious environmental challenges like global climate change and adverse health effects [1, 2]. Although CO_2 is naturally present in the atmosphere, its concentration has increased dramatically because of human activities such as fossil fuel combustion in vehicles and industries, along with large-scale deforestation [3, 4]. Among various approaches to mitigate this issue, efficiently separating CO_2 from post-combustion emissions—particularly CO_2/N_2 mixtures—remains a major challenge [5]. Consequently, it is essential to develop and refine effective methods for CO_2 capture and storage. Solid adsorbents such as metal-organic frameworks [6, 7], boron nitride (BN) nanosheets [8, 9], activated carbon [10, 11], and carbon nanotubes [12, 13] have been widely investigated due to their affordability, large surface area, and excellent selectivity. However, a common drawback is the requirement of high temperatures to release the adsorbed CO_2 during regeneration. As a result, current research efforts are focused on discovering alternative materials with better selectivity and easier regeneration processes for CO_2 capture [14, 15, 16].

In recent years, single-atom catalysts (SACs) have emerged as promising candidates for CO_2 activation due to their unique electronic structure, maximized atom utilization, and strong interaction with support materials [17, 18]. When supported on metal oxides, especially those with reducible (e.g., TiO_2, CeO_2) or irreducible (e.g., Al_2O_3, SiO_2) properties, these SACs demonstrate diverse mechanisms of CO_2 activation. In reducible oxides, oxygen vacancies and dynamic charge transfer play a crucial role in stabilizing transition metal atoms and enhancing CO_2 binding [19, 20]. On the other hand, irreducible oxides provide a more inert surface, often leading to different catalytic behavior governed by electronic modification of the active site [21]. Moreover, the application of external electric fields has recently gained attention as an effective strategy to further enhance the activation of CO_2 molecules on SACs by modulating the charge density and orbital alignment at the active site [9, 22]. Such field-induced polarization effects have shown to promote electron transfer from the SAC to the CO_2 molecule, facilitating its transformation into reactive intermediates [23]. This synergy between SACs, oxide supports, and electric field tuning offers a novel direction for the rational design of efficient CO_2 reduction catalysts.

This chapter aims to investigate the fundamental mechanisms underlying CO_2 association and dissociation processes, with a particular focus on activation strategies using single-atom catalysts (SACs) supported on reducible and irreducible metal oxides. The discussion begins by introducing the significance of CO_2 capture and activation in the context of climate change mitigation and sustainable energy conversion. It then explores the role of SACs in enhancing the adsorption and activation of CO_2 molecules at the atomic level, highlighting how the local coordination environment and the electronic structure of the support influence catalytic performance. Special attention is given to the application of external electric fields, which can modulate the charge distribution at the catalyst interface and promote bond cleavage in the CO_2 molecule. Additionally, the chapter reviews recent computational and experimental advances in tuning catalytic activity through field-assisted pathways and examines how different oxide supports affect the energetics and kinetics of CO_2 activation. These insights contribute to the rational design of next-generation catalysts

for CO_2 utilization technologies.

1.2 CO_2 Activation and Dissociation: A Thermodynamic Challenge

Carbon dioxide (CO_2) is a chemically stable and thermodynamically inert molecule, making its activation and dissociation particularly challenging [24]. This presents a major hurdle in efforts to convert CO_2 into value-added chemicals or fuels as part of carbon capture and utilization (CCU) strategies.

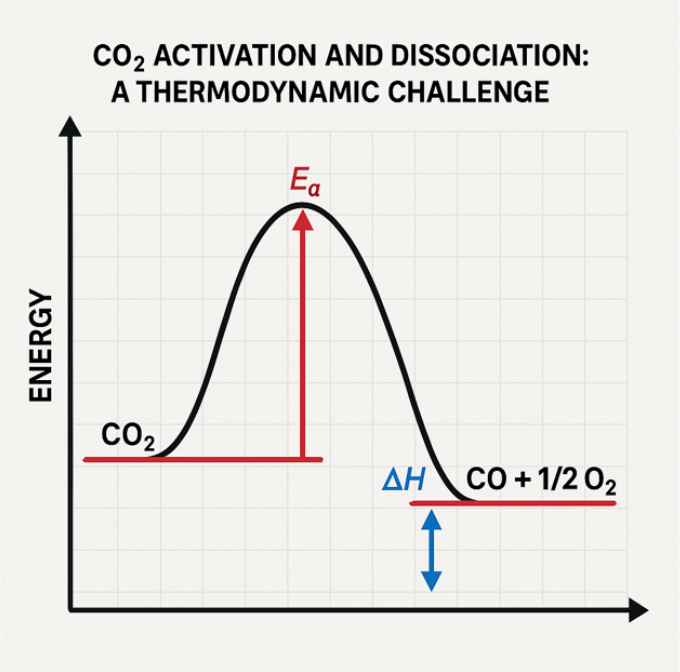

Figure 1.1: Energy profile of the CO_2 activation and dissociation reaction, illustrating the thermodynamic challenge. The reaction pathway from CO_2 to $CO + \frac{1}{2}O_2$ is endothermic, requiring significant activation energy (E_a) to overcome the energy barrier. The enthalpy change (ΔH) reflects the net energy input for the reaction.

Thermodynamic Barriers

The molecular structure of CO_2 contributes significantly to its resistance to chemical transformation. It is a linear molecule (O=C=O) with strong C=O double

bonds, each requiring approximately 750 kJ/mol to break. Additionally, CO_2 lacks a permanent dipole moment, reducing its reactivity with common reagents. From a thermodynamic perspective, CO_2 is the fully oxidized form of carbon and resides in a low-energy state. This means that any reduction process—such as converting CO_2 to carbon monoxide (CO), methane (CH_4), or methanol (CH_3OH)—requires a significant input of energy to proceed [25].

Standard Gibbs free energy changes for these transformations highlight their uphill nature:

$$CO_2 \rightarrow CO + \tfrac{1}{2}O_2 \quad \Delta G^\circ \approx +257 \text{ kJ/mol}$$
$$CO_2 \rightarrow C + O_2 \quad \Delta G^\circ \approx +394 \text{ kJ/mol}$$

These values underscore the fundamental challenge of breaking and reforming the strong chemical bonds in CO_2.

Strategies for CO_2 Activation

To overcome these energy barriers, various CO_2 activation strategies have been developed:

[label=.]**Thermal Activation**
High temperatures can provide the energy required to overcome CO_2's bond strength. However, thermal methods are energy-intensive and often lack selectivity [24]. **Catalytic Activation**
Catalysts are critical in lowering the activation energy for CO_2 conversion:

2.
- *Homogeneous catalysts* (e.g., transition metal complexes) can bind CO_2, bend its linear structure, and facilitate bond weakening.
- *Heterogeneous catalysts* (e.g., TiO_2, ZnO, CeO_2) offer surface sites where CO_2 can be adsorbed and partially activated through charge transfer or defect interactions [25].

3. **Electrochemical Reduction**

   Electrocatalysis applies an electrical potential to drive CO_2 reduction reactions (CO_2RR), enabling the formation of products like CO, HCOOH, or CH_4 under ambient conditions. While this method is promising, challenges include low selectivity, catalyst degradation, and high overpotentials.

4. **Photocatalysis**

   Photocatalytic systems harness sunlight to excite electrons in semiconductor materials. These excited electrons can transfer to CO_2 molecules and facilitate reduction reactions. This approach mimics natural photosynthesis and offers a renewable energy pathway.

5. **Plasma Activation**

   Non-thermal plasmas generate high-energy electrons that collide with CO_2 molecules, initiating bond breakage without the need for high temperatures. Plasma techniques are under active research due to their ability to activate CO_2 under mild bulk conditions.

1.3 Physisorption vs Chemisorption of CO_2 on Catalyst Surfaces

The way carbon dioxide (CO_2) interacts with catalyst surfaces plays a key role in both CO_2 capture and its chemical conversion. These interactions occur mainly through two mechanisms: physisorption and chemisorption. Understanding the differences between them is essential for designing effective materials for either temporary CO_2 storage or its activation and transformation into useful products.

Physisorption of CO_2

Physisorption refers to the weak and reversible attachment of CO_2 molecules to a surface. It is governed by non-covalent forces such as van der Waals interactions or electrostatic attraction:

- **Bonding strength:** Weak; typically less than 40 kJ/mol.
- **Molecular effect:** The CO_2 molecule remains linear and unchanged.
- **Reversibility:** Easily reversible with mild changes in pressure or temperature.
- **Surface types:** Common on porous materials like activated carbon, zeolites, and metal-organic frameworks (MOFs).
- **Applications:** Primarily used for CO_2 capture and storage, rather than for chemical reactions.

Because no chemical bond is formed, physisorption does not activate the CO_2 molecule for further reaction. However, it is useful in processes where CO_2 needs to be temporarily held or stored.

Chemisorption of CO_2

Chemisorption involves the formation of chemical bonds between CO_2 and the catalyst surface. This interaction is stronger and often leads to a change in the structure of the CO_2 molecule:

- **Bonding strength:** Strong; typically greater than 80 kJ/mol.
- **Molecular effect:** CO_2 becomes bent or partially reduced, indicating activation.
- **Reversibility:** Often irreversible under standard conditions.

- **Surface types:** Occurs on reactive surfaces like transition metals (e.g., Ni, Cu, Fe) and metal oxides (e.g., TiO_2, CeO_2).
- **Applications:** Essential for CO_2 conversion reactions, such as the formation of CO, CH_4, or CH_3OH.

Chemisorption is a critical first step in catalytic reactions that aim to convert CO_2 into fuels or other chemicals. It helps to weaken the strong C=O bonds in the molecule and allows further transformation under suitable conditions.

As described by Oura et al. (2003), physisorption is governed by weak van der Waals forces, whereas chemisorption involves stronger and often irreversible bonding between the gas molecule and the catalyst surface atoms.

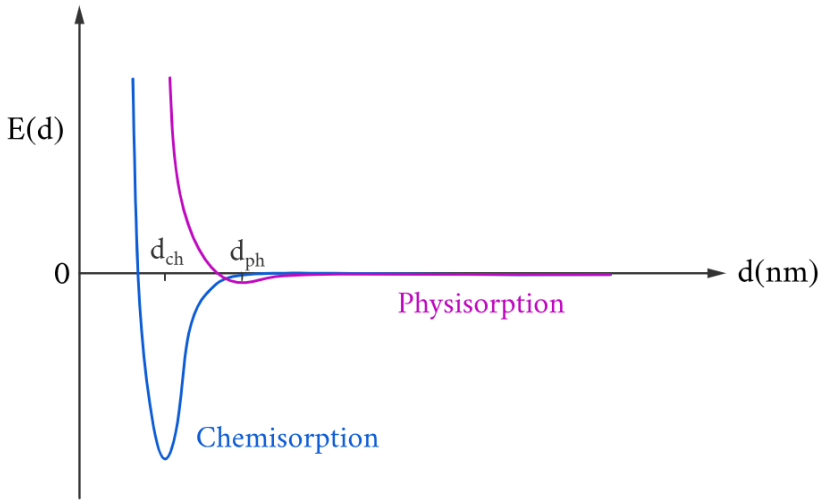

Figure 1.2: Energy-distance relationship for physisorption and chemisorption. Chemisorption (blue) occurs at shorter distance d_{ch} with deeper energy well; physisorption (magenta) occurs at longer distance d_{ph} with a shallower well.

1.4 Reducible and Irreducible Substrates in Catalysis and Plasma-Driven CO_2 Activation

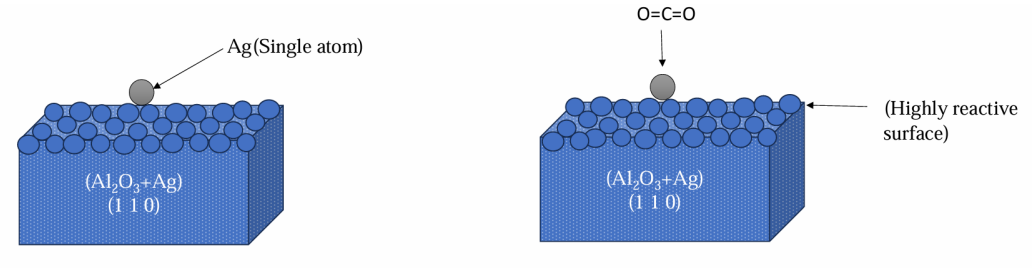

Figure 1.3: Schematic representation of a single Ag atom deposited on the $(1\bar{1}0)$ surface of an Al_2O_3 + Ag system. (Left) The Ag atom is adsorbed on the surface. (Right) CO_2 molecule interacting with the Ag site on a highly reactive surface, highlighting the potential catalytic activity.

In heterogeneous and plasma catalysis, the nature of the catalyst support—particularly its redox behavior—plays a crucial role in determining its activity and interaction with reactant molecules such as CO_2. Based on their ability to participate in redox transformations, substrates can be broadly classified into **reducible** and **irreducible** oxides.

Reducible Substrates

Reducible oxides, such as CeO_2, TiO_2, Fe_2O_3, Co_3O_4, and MnO_2, are characterized by their capacity to undergo reversible oxidation and reduction reactions. These materials readily form oxygen vacancies and exhibit mobile lattice oxygen, enabling dynamic redox cycling.

In the context of CO_2 activation, reducible substrates can facilitate electron transfer and oxygen donation/withdrawal, which are critical for breaking the strong C=O bonds in CO_2 molecules.

A notable example is ceria (CeO_2), which exhibits the Ce^{4+}/Ce^{3+} redox pair. Upon reduction, CeO_2 forms oxygen-deficient sites that can strongly adsorb and

activate CO_2, making it an excellent component in catalysts for dry reforming or plasma-assisted dissociation.

Irreducible Substrates

In contrast, irreducible oxides such as Al_2O_3, SiO_2, MgO, and, under certain conditions, ZrO_2, exhibit poor redox behavior and limited oxygen mobility. These materials do not readily form oxygen vacancies and typically serve as inert supports for catalytically active metals.

Their role in catalysis is largely structural, providing surface area and thermal stability, rather than directly participating in the activation of CO_2.

In plasma catalysis, irreducible oxides often function as dielectric supports in dielectric barrier discharge (DBD) systems. Although they contribute minimally to chemical activation, they influence plasma properties, such as electric field distribution and surface charge accumulation.

Doherty and Goldsmith (2023) modeled the plasma-induced surface charge effects on CO_2 activation by single atom catalysts supported on both reducible and irreducible oxides, showing the crucial role of substrate type in plasma-enhanced catalytic systems [26].

CONCEPTS AND COMPUTATIONAL METHODOLOGY

Chapter 2

CONCEPTS AND COMPUTATIONAL METHODOLOGY

2.1 Approximation Method

In the realm of quantum mechanics, our aim is to derive a wavefunction that encapsulates all pertinent details regarding the quantum system under investigation. This system could range from a simple free particle, a particle confined in a box, a slightly intricate harmonic oscillator, to more complex entities like the hydrogen atom, helium atom, hydrogen ion, and even more elaborate structures such as molecules, quantum dots, nanotubes, quasi-two dimensional sheets, or crystals. Extracting information from this wavefunction entails solving Schrödinger's equation, which represents the full Hamiltonian of the system, encompassing all interactions within the quantum domain.

Considering a solid, we envision it as comprising N heavy, positively charged nuclei and ZN lighter, negatively charged electrons. This configuration presents us with a quantum many-body problem with N+ZN interacting particles, and the corresponding many-particle Hamiltonian is articulated as follows:

$$\hat{H} = \frac{-\hbar^2}{2}\sum_i \frac{\nabla^2_{\vec{R}_i}}{M_i} - \frac{\hbar^2}{2}\sum_i \frac{\nabla^2_{\vec{r}_i}}{m_e} - \frac{1}{4\pi\epsilon_0}\sum_{i,j}\frac{e^2 Z_i}{|\vec{R}_i - \vec{r_j}|} + \frac{1}{8\pi\epsilon_0}\sum_{i\neq j}\frac{e^2}{|\vec{r_i} - \vec{r_j}|} + \frac{1}{8\pi\epsilon_0}\sum_{i\neq j}\frac{e^2 Z_i Z_j}{|\vec{R}_i - \vec{R}_j|} \tag{2.1}$$

The mass of the nucleus at $\vec{R}_i$ is M_i , the electrons have mass m_e and are at $\vec{r_i}$ .The first two terms in the Hamiltonian correspond to the kinetic energy operators for nuclei and electrons, respectively. The subsequent terms delineate the Coulombic interactions among electrons and nuclei, electrons among themselves, and nuclei with each other. However, solving this comprehensive Hamiltonian exactly is infeasible. Nonetheless, through a series of approximations, we can derive acceptable approximate eigenstates, facilitating the extraction of various insights about the system.

2.2 The Born-Oppenheimer approximation

In this approximation, we opt to immobilize the N nuclei at their respective positions due to their significantly greater mass and reduced mobility compared to electrons. Consequently, our many-body problem now revolves solely around the behavior of electrons. The fixed nuclei serve as the 'external' entities relative to the electron cloud.

Upon implementing this approximation, the many-body problem transforms into a many-electron system. Herein, we contend with a cohort of NZ interacting electrons, navigating within the given potential field created by the immobilized nuclei.

After fixing the ionic coordinates R_i in space, the simplified Hamiltonian for electrons, adhering to the Born-Oppenheimer approximation, is delineated as:

$$\hat{H} = -\hbar^2/2\sum_i \frac{\nabla^2_{\vec{r}_i}}{m_e} - \frac{1}{4\pi\epsilon_0}\sum_{i,j}\frac{e^2 Z_i}{|\vec{R}_i - \vec{r_j}|} + \frac{1}{8\pi\epsilon_0}\sum_{i\neq j}\frac{e^2}{|\vec{r_i} - \vec{r_j}|} \tag{2.2}$$

It's crucial to note that in this formulation, we haven't accounted for electron-phonon scattering or temperature effects, as our focus remains on describing the Hamiltonian

for a solid. Formally, we express this as:

$$\hat{H} = \hat{T} + \hat{V_{ext}} + \hat{V} \tag{2.3}$$

Here, the Hamiltonian encompasses solely the kinetic energy of the electron gas ($\hat{T}$), the potential energy attributed to electron-electron interactions ($\hat{V}$) and the potential energy of electrons in the now external potential field of the immobilized nuclei ($\hat{V_{ext}}$).

2.3 Density Functional Theory Approach

After applying the Born-Oppenheimer approximation, the resultant quantum many-body problem, represented by equation (2.2), is notably simpler compared to its original form, equation (2.1). Nonetheless, solving it exactly remains exceedingly challenging. To tackle this complexity, various methods aim to further simplify equation (2.2) into a more manageable and approximate format. Among these, the *Thomas-Fermi model* and the *Hartree-Fock model*,hold paramount importance and are extensively discussed in condensed matter physics [27].

The *T-F model* marks the pioneering attempt to utilize electron density as a variable, paving the way for subsequent developments. Following this, the *H-F method* emerges as a more sophisticated approximation, grounded in the self-consistent field approach. This method hinges on assumptions aligned with the independent particle approximation and the Pauli exclusion principle. Its framework finds considerable utility in the realm of atoms and molecules, hence extensively employed in quantum chemistry. However, its accuracy diminishes when applied to solids.

In our discussion, we will delve into a more contemporary and robust approach: Density Functional Theory (DFT).

2.3.1 The Theorems of Hohenberg and Kohn

In 1964, Hohenberg and Kohn introduced two fundamental theorems that form the bedrock of Density Functional Theory (DFT), elucidating the relationship between electron density and the external potential. These theorems are as follows[28]:

First theorem: ***"The external potential V(r) is a unique functional of the electron density n(r) i.e F[n(r)]. As a result the total ground state energy E of any system is also unique functional of n(r, E=E[n(r)])."***

Second Theorem: ***"The functional E[n] for the total energy has a minimum equal to that ground state energy at ground state density."***

Expanding upon the aforementioned theorems:

The ground state energy of a system comprising interacting electrons in an external field (Vn($\mathbf{r}$)) can be expressed as a unique functional, denoted as F[n($\mathbf{r}$)], of the single-particle electron density, n($\mathbf{r}$)":

$$E[n(\vec{\mathbf{r}})] = F[n(\vec{\mathbf{r}})] + \int V(\vec{\mathbf{r}})n(\vec{\mathbf{r}})\, d^3r \tag{2.4}$$

$$F[n(\vec{\mathbf{r}})] = T_0[n] + \frac{1}{2}\iint \frac{e^2}{4\pi\epsilon_0}\frac{n(\vec{\mathbf{r}'})n(\vec{\mathbf{r}})}{|\vec{r}-\vec{r'}|}\, d^3r\, d^3r' + E_{XC}[n] \tag{2.5}$$

Where $T_0[n]$ is the kinetic energy of non-interacting electrons , the senond term is the classical coulomb energy and E_{XC} exchange correlation energy. The functional $E[n(\vec{\mathbf{r}})]$ is minimum at the equilibrium density $n_0(\vec{r})$ according to the variation $\delta n(\vec{r})$:

$$\left.\frac{\delta E[n(\vec{\mathbf{r}})]}{\delta n(\vec{\mathbf{r}})}\right|_{n=n_0} \tag{2.6}$$

Understanding the properties of ground-state density $n_0(\vec{r})$ in a multi electron system:

1."A direct implication of the one-to-one correspondence between the ground-state density $n_0(\vec{r})$ of a many-electron system (such as an atom, molecule, or solid) and the external potential V_{ext} is the uniqueness of the ground-state expectation value of any observable $\hat{O}$. This implies that the expectation value of any observable in the ground state is solely determined by the exact ground-state electron density. "

$$< \Psi|\hat{O}|\Psi >= O[\rho] \tag{2.7}$$

2."For $\hat{O}$ being the hamiltonian $\hat{H}$, the ground-state total energy functional $H[\rho] = E_{V_{ext}}[\rho]$ is of the form"

$$\begin{aligned} E_{V_{ext}}[\rho] &= \underbrace{< \Psi|\hat{T} + \hat{V}|\Psi >}_{F_{HK}[\rho]} + < \Psi|\hat{V_{ext}}|\Psi > \\ &= F_{HK}[\rho] + \int \rho(\vec{r}) V_{ext}(\vec{r}) d\vec{r} \end{aligned} \tag{2.8}$$

Here $F_{HK}[\rho]$represents the Hohenberg-Kohn density functional, which exhibits a **universal** nature applicable to any multi-electron system. The functional $E_{V_{ext}}[\rho]$ achieves its minimum value, equivalent to the ground-state total energy, when evaluated for the ground-state density corresponding to the external potential V_{ext} .

We will examine three fundamental consequences of the Hohenberg-Kohn density functional l $F_{HK}[\rho]$: invertibility (establishing a one-to-one correspondence $\rho \leftrightarrow V_{ext}$),universality, and the variational property (minimal value).

Firstly, for a given many-electron system, there exists a singular external potential V_{ext} , and solving the Hamiltonian equation (2.2) and Schrödinger's equation for this specific V_{ext} leads to a unique ground-state wave function for the many-particle system. From this wave function, we can straightforwardly compute the corresponding

electron density. The first theorem of Hohenberg and Kohn guarantees the uniqueness of this calculated electron density for the given V_{ext} and vice-versa.It's essential to note that the density encapsulates as much information as the wave function, not less. All observable quantities can be uniquely derived from the density alone, expressed as functionals of the density. This establishes the one-to-one correspondence between the electron density ρ and and the external potential V_{ext}.

Second, the universality of $F_{HK}[\rho]$ arises from its independence regarding information on the nuclei and their positions. As a result, $F_{HK}[\rho]$ serves as a universal functional applicable to any many-electron system. The functional form of $F_{HK}[\rho]$ is expressed as:

$$F[n(r)] = T_0[n] + \frac{1}{2}\frac{e^2}{4\pi\epsilon_0}\iint \frac{n(r)n(r')}{|r-r'|}d^3r d^3r' + E_{XC}[n] \tag{2.9}$$

Here, the first term denotes the kinetic energy of a non-interacting electron gas of density n[r]. The second term represents the classical Coulomb energy, while the third term accounts for the exchange-correlation energy. Consequently, an expression for $F_{HK}[\rho]$ exists in principle, applicable to every conceivable atom, molecule, or solid. This universality underscores the versatility and broad applicability of the Hohenberg-Kohn density functional.

Thirdly, the second theorem facilitates the utilization of the variational principle, such as the Rayleigh-Ritz method, to determine the ground-state density. Out of the infinite potential densities, the one that minimizes the functional $E_{V_{ext}}[\rho]$ corresponds to the ground-state density for the external potential $V_{ext}(\vec{r})$. This process relies on the approximate knowledge of $F_{HK}[\rho]$. By employing this theorem, one can efficiently identify the ground-state density, a crucial step in understanding the electronic structure and properties of complex systems.

2.3.2 The Kohn-Sham equation

The equations formulated by Kohn and Sham in 1965 marked a pivotal moment, transforming Density Functional Theory (DFT) into a practical computational tool [29]. They introduced two key energy functionals, $E_e[\rho]$ and $E_{HF}[\rho]$ associated with the exact and Hartree-Fock Hamiltonians, respectively.

$$E_e = T + V \tag{2.10}$$

$$E_{HF} = T_0 + \underbrace{V_H + V_x}_{\text{V}} \tag{2.11}$$

where T is the exact (true) kinetic energy functional and V is exact electron-electron potential energy functional , T_0 is the kinetic energy functional for the non-interacting electron gas, V_H is the Hartree contribution and V_x is the exchange contribution. The functional for the correlation contribution is:

$$V_c = T - T_0 \tag{2.12}$$

The fraction of total energy present in the Hartree-Fock solution but absent in the Hartree solution constitutes the exchange contribution. The Hartree functional, is given by:

$$E_H = T_0 + V_H \tag{2.13}$$

It can be written as

$$V_x = V - V_H \tag{2.14}$$

Now rewriting the Hohenberg-Kohn functional from the above idea:

$$\begin{aligned} F_{HK} &= T + V + T_0 + T_0 \\ &= T_0 + V + \underbrace{(T - T_0)}_{\text{Vc}} \\ &= T_0 + V + V_c + V_H - V_H \\ &= T_0 + V_H + V_c + \underbrace{(V - V_H)}_{\text{Vx}} \\ &= T_0 + V_H + \underbrace{V_x + V_C}_{\text{Vxc}} \end{aligned}$$

Here The V_{XC} is the exchange-correlation energy fuctional . Assuming we know V_{XC} , we can explicitly write the energy functional:

$$E_{V_{ext}}[\rho] = T_0[\rho] + V_H[\rho] + V_{xc}[\rho] + V_{ext}[\rho] \tag{2.15}$$

So, the expression can be interpreted as the energy functional of a non-interacting classical electron gas influenced by two external potentials: one arising from the nuclei and the other stemming from the exchange-correlation effect. The corresponding Hamiltonian, known as the Kohn-Sham Hamiltonian, is formulated as:

$$\hat{H_{KS}} = \hat{T_0} + \hat{V_H} + \hat{V_{xc}} + \hat{V_{ext}} \tag{2.16}$$

i.e,

$$\hat{H_{KS}} = -\frac{\hbar^2}{2m_e}\vec{\nabla_i^2} + \frac{e^2}{4\pi\epsilon_0}\int \frac{\rho(\vec{r'})}{|\vec{r} - \vec{r'}|}d\vec{r'} + V_{xc} + V_{ext} \tag{2.17}$$

Where the exchange -correlation potential is given by the functional derivative ,

$$\hat{Vxc} = \frac{\delta V_{xc}}{\delta \rho} \tag{2.18}$$

The K-S equation in the eigen value form:

$$\left[-\frac{\hbar^2}{2m_e}\nabla^2 + V_{ext}(\vec{r}) + V_H(\vec{r}) + V_{xc}(\vec{r})\right]\phi_i(\vec{r}) = \epsilon_i\phi_i(\vec{r}) \tag{2.19}$$

i.e,

$$\left[-\frac{\hbar^2}{2m_e} + V_{eff}\right]\phi_i(\vec{r}) = \epsilon_i\phi_i(\vec{r}) \tag{2.20}$$

This equation is known as the Kohn-Sham equation and $\phi_i(\vec{r})$ is the Kohn-Sham states, ϵ_i is the Kohn-Sham energy, and V_{eff} is the Kohn-Sham potential.

So the exact ground state density $\rho(\vec{r})$ of an N- electron system from single particle is

$$\rho(\vec{r}) = \sum_{i=1}^{N} \phi_i(\vec{r}) * \phi_i(\vec{r}) \tag{2.21}$$

It's crucial to note that the single-particle wave functions ϕ_i do not represent the wave functions of individual electrons; instead, they describe mathematical quasi-particles lacking direct physical interpretation. However, the aggregate density of these quasi-particles is ensured to match the true electron density. Similarly, the single-particle energies ϵ_i should not be misconstrued as energies pertaining to individual electrons.

Both the Hartree operator V_H and the exchange-correlation operator V_{xc} depend on the density $\rho(\vec{r})$, which, in turn, is dependent on the single-particle wave functions ϕ_i being sought. This dependence creates a self-consistency problem, as we're stuck in a loop: the solutions (ϕ_i) determine the original equation(V_H and V_{xc} in H_{KS}),yet the equation cannot be formulated and solved until its solution is known. To overcome this challenge, a self-consistent method is employed, iteratively carried out on a computer as depicted in Figure 2.1.

Initially, an educated guess is made regarding the form of the single-particle wave functions $\phi_i(\vec{r})$ from which an initial electron density $\rho(\vec{r})$ is constructed. This constructed density is then utilized to formulate the Kohn-Sham Hamiltonian (H_{KS}). Solving the eigenvalue problem yields a new set of single-particle wave functions (ϕ_i) from which a new electron density ($\rho(\vec{r'})$) is determined.This iterative process is repeated until the density converges, ensuring consistency with the Hamiltonian.

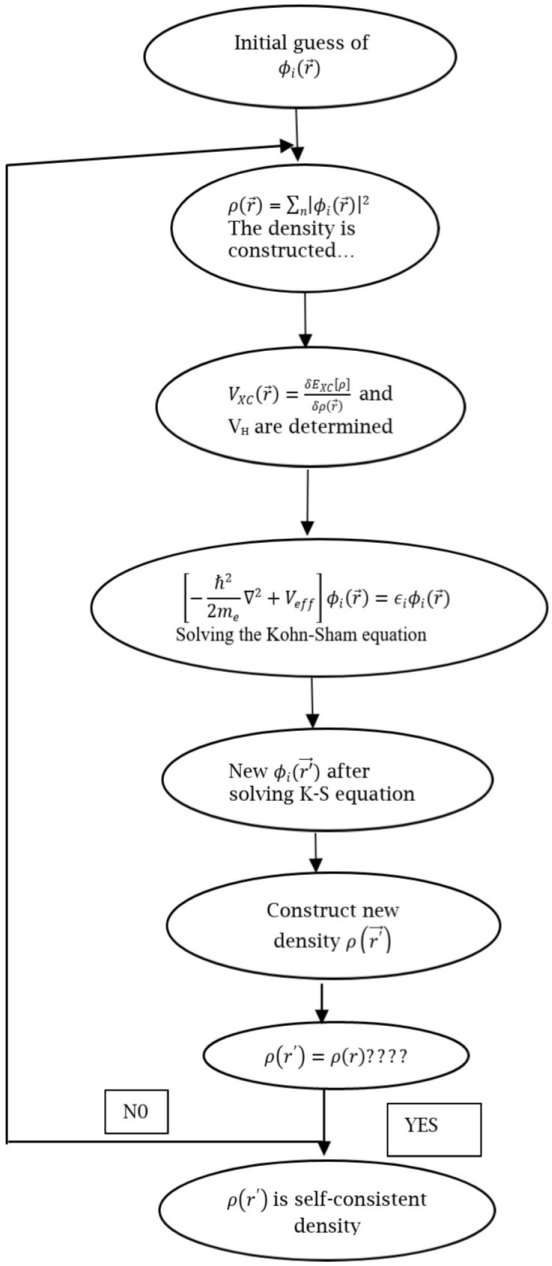
Initial guess of $\phi_i(\vec{r})$
$\rho(\vec{r}) = \sum_n |\phi_i(\vec{r})|^2$ The density is constructed...
$V_{XC}(\vec{r}) = \frac{\delta E_{XC}[\rho]}{\delta \rho(\vec{r})}$ and V_H are determined
$\left[-\frac{\hbar^2}{2m_e}\nabla^2 + V_{eff}\right]\phi_i(\vec{r}) = \epsilon_i \phi_i(\vec{r})$ Solving the Kohn-Sham equation
New $\phi_i(\vec{r'})$ after solving K-S equation
Construct new density $\rho(\vec{r'})$
$\rho(r') = \rho(r)????$
N0
YES
$\rho(r')$ is self-consistent density

Figure 2.1: Flow chart for the scf calculation to solve Kohn-Sham equations.

2.3.3 The exchange-correlation functional

The primary challenge posed by Equation 2.19 is the lack of exact knowledge regarding the exchange-correlation potential V_{xc} or the corresponding exchange-correlation energy (E_{xc}).However, various approximations have been developed to address this issue, such as the Local Density Approximation (LDA), Generalized Gradient Approximation (GGA), meta-GGA, Hybrid-functional, and RPA/GW methods. For the scope of our discussion, we will focus on GGA and LDA.

The efficacy of Density Functional Theory (DFT) crucially hinges on the accuracy of the exchange-correlation functional employed to solve the Hamiltonian. Therefore, the choice of approximation method greatly impacts the quality of DFT predictions.

Local Density Approximation

A commonly utilized approximation in Density Functional Theory (DFT) is the Local Density Approximation (LDA). In LDA, it is assumed that the exchange-correlation energy density at each position within a molecule is equivalent to that of a Uniform Electron Gas (UEG) with the same density as observed at that position. Mathematically, this is expressed as:

$$E_{xc}^{LDA}[\rho] = E_{x}^{LDA}[\rho] + E_{c}^{LDA}[\rho] \tag{2.22}$$

The expression for exchange energy is simple

$$E_{x}^{LDA}[\rho] = C \int \rho^{\frac{4}{3}}(\vec{r}) d\vec{r} \tag{2.23}$$

Various expressions for the correlation energy $E_{xc}^{LDA}[n]$ have been derived by fitting to the outcomes of accurate Quantum Monte Carlo (QMC) calculations for the UEG. Thus, the exchange-correlation functional takes the form:

$$E_{xc}^{LDA}[\rho] = \int \rho(\vec{r}) \epsilon_{xc}(\rho(\vec{r})) d\vec{r} \tag{2.24}$$

Generalised Gradient Approximation

An enhancement in accuracy beyond that provided by LDA can be achieved through Generalized Gradient Approximation (GGA) functionals. Unlike LDA, GGA functionals depend not only on the value of the electron density at a point but also on its gradient. Therefore, we have:

$$E_{xc}^{GGA}[\rho] = \int \rho(\vec{r})\epsilon_{xc}(\rho(\vec{r}), |\nabla\rho(\vec{r})|)d\vec{r} \tag{2.25}$$

Most GGA functionals are formulated as a correction term added to the LDA functional:

$$\epsilon_{x/c}^{GGA}[\rho] = \epsilon_{x/c}^{LDA}[\rho] + \Delta\epsilon_{x/c}\left[\frac{|\nabla\rho(\vec{r})}{\rho^{4/3}(\vec{r})}\right] \tag{2.26}$$

2.3.4 Spin-Orbit Interaction

Spin-orbit coupling (SOC) refers to the interaction between an electron's spin magnetic moment and its orbital angular momentum. In solids, SOC leads to the lifting of degeneracy among one-electron levels. This effect is particularly pronounced in materials containing heavy elements such as **Pb**, **I**, or **Bi**, where relativistic effects significantly influence electron behavior. Consequently, solving the relativistic Dirac equation becomes necessary to accurately account for SOC.

However, as an initial approximation, the non-relativistic Kohn-Sham equation can be employed by introducing a spin-dependent term in the Hamiltonian:

$$\left[-\frac{1}{2}\nabla^2 + V_{ext}(\mathbf{r}) + V_H(\mathbf{r}) + V_{xc}(\mathbf{r}) + \mu_B\sigma.B_{xc}(\mathbf{r})\right]\phi_i(\mathbf{r}) = \epsilon_i\phi_i(\mathbf{r}) \tag{2.27}$$

where μ_B is the Bohr magneton, B_{xc} is the exchange and correlation magnetic field, and σ is the matrix vector defined by:

$$\sigma = \sigma_x u_x + \sigma_y u_y + \sigma_z u_z \tag{2.28}$$

Where $\sigma_x, \sigma_y, \sigma_z$ are Pauli matrices and u_x, u_y, u_z are the unit vectors along the x, y

and z direction.The spin calculations can be conducted in either a collinear or non-collinear manner. The collinear approach assumes that spin densities align in the same direction. To incorporate SOC effects, a non-collinear spin calculation can be performed using packages like Quantum ESPRESSO (QE).

2.4 Solving the equations

In either the approximation of Hartree-Fock (HF) or Density Functional Theory (DFT), the result yields an infinite sequence of one-electron equations of the following form (where m is an integer that counts the members of the set):

$$\underbrace{\left[-\frac{\hbar^2}{2m_e}\vec{\nabla}_m^2 + \frac{e^2}{4\pi\epsilon_0}\int\frac{\rho(\vec{r'})}{|\vec{r}-\vec{r'}|}d\vec{r'} + V_\alpha + V_{ext}\right]}_{H_{sp}}\phi_m(\vec{r}) = \epsilon_m\phi_m(\vec{r}) \tag{2.29}$$

Here the H_{sp} is the single particle Hamiltonian. For Hartree-Fock , V_α is the exchange operator. The ϕ_m are true one-electron (or single-particle) orbitals for HF. In HF, the exchange is treated exactly, but correlation effects are not incorporated at all.

For DFT, V_α represents the exchange-correlation operator , which is approximated in methods like LDA, GGA, or others. In DFT, both exchange and correlation effects are treated, albeit approximately. The ϕ_m represent mathematical quasi single-particle orbitals. The resemblance between the Hartree-Fock and Kohn-Sham equations allows for the use of similar mathematical techniques to solve them. Typically, "solving" entails finding the coefficients c_p^m needed to express ϕ_m in a given basis set ϕ_p^b :

$$\phi_m = \sum_{p=1}^{P} c_p^m \phi_p^b \tag{2.30}$$

The wave functions ϕ_m are theoretically infinite, as m belongs to a function space with infinite dimensions. Thus, P is infinite. In practice, only a limited number of basis functions are employed. Although such a restricted basis may not perfectly represent ϕ_m, it is still possible to construct a basis that can generate a function that

closely resembles ϕ_m. Substituting over two conditions, we get:

$$\begin{bmatrix} ... & ... & ... \\ | & \langle \phi_i^b | \hat{H} | \phi_j^b \rangle - \epsilon_m \langle \phi_i^b | \phi_j^b \rangle & | \\ ... & ... & ... \end{bmatrix} \begin{bmatrix} c_1^m \\ | \\ c_P^m \end{bmatrix} = \begin{bmatrix} 0 \\ | \\ 0 \end{bmatrix}$$

Diagonalizing the Hamiltonian matrix will yield P eigenvalues and P sets of coefficients for each of the P eigenfunctions in the specified basis (for more eigenfunctions). The larger P, the better the eigenfunction approximation, but it also increases the computational complexity of matrix diagonalization on classical computers.

2.5 Applications of DFT

2.5.1 Equilibrium Structure

Atomic forces

In standard DFT, the nuclei are treated as classical particles, allowing us to utilize Newton's equations for their dynamics. The total force acting on each atom can be determined using classical mechanics:

$$F_I = -\frac{\partial U}{\partial R_I} \tag{2.31}$$

where F_I is the force on I-th nucleus and U is the total potential energy. However, directly calculating $\frac{\partial U}{\partial R_I}$ is challanging. Although the finite displacement method is an option, it's highly time-consuming. Alternatively, the Hellmann-Feynman theorem offers a solution by employing first-order perturbation theory:

$$F_I = -\langle \Psi | \frac{\partial H}{\partial R_I} | \Psi \rangle - \frac{\partial V_{NN}}{\partial R_I} \tag{2.32}$$

where V_{NN} is the classical potential energy of nuclei. The second term in Eq. 2.32 accounts for the electrostatic field of the nuclei.

Ionic Optimization

Once the atomic forces on each atom are established, structural optimization can proceed using various algorithms such as conjugate gradient (CG), quasi-Newton, and damped molecular dynamics. The equilibrium structure can be attained by initiating with an initial guess of atomic positions, followed by computing the electron density and energy through Kohn-Sham self-consistent calculations. This step is known as the electronic step. Subsequently, the atomic force on each atom can be determined using Equation 2.32. New atomic positions can then be obtained employing an algorithm like CG. These updated atomic positions serve as a new starting point for the cycle, referred to as the ionic step. The termination condition for the loop can be chosen based on either the atomic forces and stress or the energy of the entire structure.

2.5.2 Band Structures and Density of States (DOS)

After solving the periodic Kohn-Sham equation (Eq. 2.20), the energy states, known as Kohn-Sham states, can be obtained. The total energy from Eq. 2.20 is given by:

$$E = \frac{1}{\Omega_{BZ}} \sum_{n} \int_{BZ} f_{n\mathbf{k}} \epsilon_{n\mathbf{k}} d\mathbf{k} - \int V_{xc}(\mathbf{r}) n(\mathbf{r}) d\mathbf{r} - E_H + E_{xc} \tag{2.33}$$

Here, the first term represents the band structure energy, and the subsequent terms account for the double counting inherent in the first term. The electronic density of states (DOS) can be calculated as:

$$\rho(E) = \frac{1}{\Omega} \sum_{n} \int_{BZ} d\mathbf{k} \delta(E - \epsilon_{n\mathbf{k}}) \tag{2.34}$$

where $\rho(E)dE$ denotes the number of Kohn-Sham states between energy levels E and E+dE. The band structure and DOS are valuable tools for analyzing the

electronic structure. Additionally, besides the total DOS, partial density of states can be determined for each orbital.

2.6 Computational Package

2.6.1 VASP

VASP (Vienna Ab-initio Simulation Package) is a computational simulation tool that employs Density Functional Theory (DFT) to provide a diverse array of material properties, such as total energy, electronic density of states, band structure, and lattice parameters. One of the primary benefits of utilizing VASP is its capability to deliver highly accurate electronic structures. Additionally, VASP boasts scalability, enabling its utilization across a broad spectrum of computer systems, ranging from small-scale to large-scale computing platforms.

INPUT FILES

To initiate a calculation in VASP, a set of input files is necessary to compute various properties associated with the material under investigation.

The essential input files for running a VASP calculation include:

1. INCAR - This file contains critical settings for the VASP calculation, encompassing parameters like calculation type, convergence criteria, and electronic configurations.

2. POSCAR - This file encapsulates the crystal structure of the material being simulated, detailing atomic positions and lattice vectors.

3. POTCAR - This file holds the pseudopotentials utilized to characterize the electron-ion interactions within the material.

4. KPOINTS - This file delineates the k-point sampling utilized in the calculation.

Accurate and reliable calculations hinge upon the meticulous setup of these input files. VASP offers a plethora of tools and comprehensive documentation to aid users in configuring input files accurately.

OUTPUT FILES

When conducting a calculation with VASP, several output files are generated, each providing valuable information about the computation:

1. OUTCAR - This file furnishes comprehensive details regarding the calculation, encompassing convergence criteria, the number of electronic and ionic steps taken, and the final total energy attained.

2. OSZICAR - This file offers a condensed summary of the ionic steps taken during the calculation, along with the final total energy achieved.

3. vasprun.xml - This XML-formatted file presents an overview of the entire computation, featuring crucial data such as the total energy, electronic density of states, and band structure.

4. CHG, CHGCAR - These files contain the charge density distribution of the system, which can be visualized using specialized visualization software to gain insights into the electronic structure.

5. WAVECAR - This file holds the wavefunctions of the system, allowing for the calculation of additional properties or the resumption of a calculation from a specific point.

In addition to these primary output files, VASP may generate various other files depending on the specific nature of the computation being performed. For instance, in phonon calculations, a FORCE CONSTANTS file may be produced, detailing the

force constants of the system.

2.6.2 LAMMPS

LAMMPS (Large-scale Atomic/Molecular Massively Parallel Simulator) is a powerful molecular dynamics simulation software capable of simulating a wide range of materials and systems at the atomic scale. One of the key functionalities of LAMMPS is its ability to perform relaxation simulations, which are essential for studying the equilibrium structures and properties of materials under various conditions.

LAMMPS, stands out for its comprehensive capabilities in atomistic simulations. Treating each atom as an individual entity, it meticulously models interatomic interactions using a diverse array of potential models, from classical force fields like Lennard-Jones and Tersoff potentials to specialized ones tailored for specific materials and applications. Its high degree of parallelization enables efficient utilization of computational resources across multiple processors or computing nodes, facilitating simulations of large-scale systems and expediting relaxation calculations. LAMMPS excels in dynamical relaxation simulations, guiding systems through iterative energy minimization and molecular dynamics steps until reaching equilibrium, thereby offering invaluable insights into structural and thermodynamic properties.

2.6.3 SIESTA

SIESTA (Spanish Initiative for Electronic Simulations with Thousands of Atoms) is a widely used computational simulation tool based on Density Functional Theory (DFT) for studying the electronic structure of materials. Developed by the Spanish National Research Council (CSIC), SIESTA provides an efficient and accurate approach to investigate a variety of material properties, including total energy, electronic density of states, band structure, and atomic forces. SIESTA is recognized for its efficiency in handling large-scale simulations involving thousands of atoms, making it suitable for studying systems with complex structures or interfaces. It offers

flexibility in choosing the level of theory and the type of basis sets, allowing users to tailor simulations according to their specific research needs. SIESTA employs localized atomic orbitals as basis sets, resulting in computational efficiency and enabling simulations of systems with high precision. Additionally, SIESTA is parallelized, enabling efficient utilization of computational resources across multiple processors or computing nodes, thereby reducing the simulation time for large-scale calculations.

INPUT FILES

Similar to VASP, initiating a simulation in SIESTA requires a set of input files, including:

1. Input File (input.fdf): This file contains parameters for the simulation, such as calculation type, convergence criteria, and system setup details.
2. Pseudopotential Files (input.psf) : SIESTA utilizes pseudopotentials to approximate the electron-ion interactions within the material, which are specified in separate files.

OUTPUT FILES

Upon completion of a simulation, SIESTA generates several output files, including:

1. Output Log File: This file provides detailed information about the simulation process, including convergence criteria, the number of electronic and ionic steps, and the final total energy.
2. Electronic Density File: SIESTA produces files containing electronic density distributions, which can be visualized to analyze the electronic structure of the material.
3. Band Structure and Density of States Files: SIESTA generates files containing

information about the electronic band structure and density of states, facilitating analysis of the material's electronic properties.

4. Force and Stress Files: SIESTA provides files containing information about atomic forces and stresses, which are crucial for understanding mechanical and structural properties.

Generation of SIESTA Input Files through Iterative Visualization Processes

For generating SIESTA input files we have used a sequential process involving multiple visualization tools. Beginning with a relaxed structure obtained from LAMMPS simulations, the lammps.dat.min file is subjected to visualization in OVITO software for initial analysis. Subsequently, the structure is exported as a .cif file for further refinement in Burai, where adjustments are made to ensure proper centering of layer in z direction. Following this, the centered structure is exported once more as a POSCAR file and imported into WXDragon for the finalization of the SIESTA input file. This iterative approach harnesses the capabilities of each visualization tool to refine the atomic structure iteratively, culminating in the creation of an accurate and optimized SIESTA input file for subsequent computational simulations.

Electronic Structure and Interaction Analysis of Single Metal Atoms on Al_2O_3 Surface

Chapter 3

Electronic Structure and Interaction Analysis of Single Metal Atoms on Al_2O_3 Surface

3.1 Structure

In this section, we describe the structural models used to investigate the interaction of single metal atoms with the Al_2O_3 surface. TheAl_2O_3 slab was modeled using a periodic supercell, and metal atoms were adsorbed on top of the surface in various configurations. Structural optimizations were performed to obtain relaxed geometries before proceeding to electronic structure and interaction energy calculations.

3.1.1 Al_2O_3-Ag-CO_2 Configuration

The first structure consists of a silver (Ag) atom deposited on anAl_2O_3 surface with a CO_2 molecule nearby. The system contains 63 atoms in total: 22 aluminum, 39 oxygen, 1 silver, and 1 carbon. The optimized atomic positions were extracted from the VASP-generated POSCAR file.

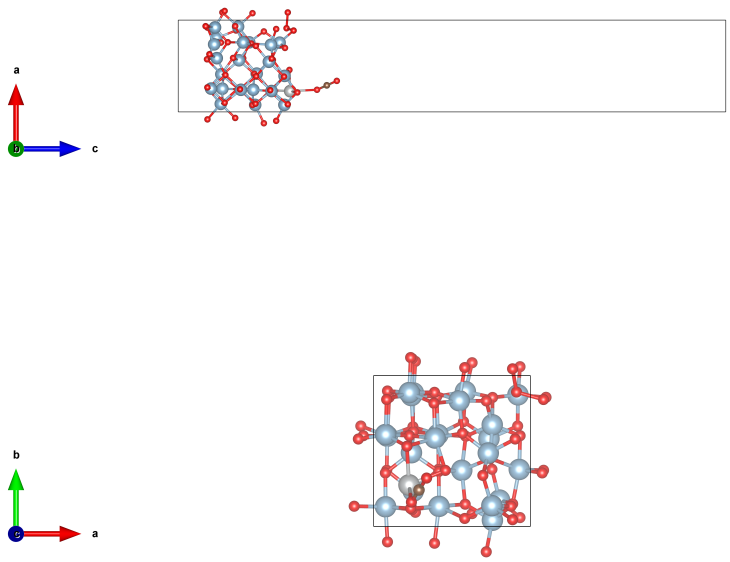

Figure 3.1: Side and Top views of the relaxed Al_2O_3-Ag-CO_2 structure visualized using VESTA.

Table 3.1: Structural parameters of the investigated systems

Structure Name	**Bravais Lattice**	**Cell Dimensions**
Al_2O_3 + Co + CO_2	Tetragonal	$a = 8.37239$ Å, $b = 8.04428$ Å, $c = 50$ Å, $\alpha = 90°$, β
Al_2O_3 + Cu + CO_2	Tetragonal	$a = 8.37239$ Å, $b = 8.04428$ Å, $c = 50$ Å, $\alpha = 90°$, β
Al_2O_3 + Ag + CO_2	Tetragonal	$a = 8.37239$ Å, $b = 8.04428$ Å, $c = 50$ Å, $\alpha = 90°$, β

The corresponding POSCAR file is included below for reference:

```
Generated by ATOMKIT code
1.0
        8.3723897934          0.0000000000          0.0000000000
        0.0000000000          8.0442800522          0.0000000000
        0.0000000000          0.0000000000         50.0000000000
   Al    O   Ag    C
   22   39    1    1
Cartesian
     6.724539853          1.405085973          3.487492725
```

2.017177763	6.978031340	5.726992711
2.021092180	3.932801336	6.850925088
6.158917524	4.681716948	3.280557320
6.343551369	0.330133684	6.481510401
2.124268816	7.117193147	2.998080850
6.334428041	5.419700256	5.925902352
2.116545277	1.883209345	4.030563682
0.731411928	4.814820570	3.887793794
4.707427214	2.993227905	5.546326190
7.777301542	3.038653505	5.467730388
3.435298463	4.899178220	3.938133642
4.900454301	7.191089579	3.522459418
0.639966567	1.048852588	7.029391825
3.492448008	1.071948729	7.167919725
7.706143882	7.017531569	3.361906111
6.313560464	1.108669673	9.261488914
6.122863365	3.914494925	8.468158543
1.904103550	7.137145122	8.523736149
0.640637829	4.899794826	9.695632756
3.282502195	4.713827965	9.709922969
4.572063927	6.703499424	8.276109397
7.630920598	7.166459833	9.891375899
6.014827641	6.692226932	7.085612416
2.232889157	0.755124412	2.663004212
2.125758431	5.056449374	5.448491126
6.319408636	3.048899197	3.898810223
6.350753417	6.876488295	4.526720196
2.059700392	0.898959138	5.646477267
2.100037006	5.310896021	2.743925899
6.237722370	3.628116824	6.669447571
3.252348606	7.149806656	7.112260908

7.816991159	0.471856405	2.500000037
5.258629976	0.684152068	2.848140523
0.741864056	7.221719494	7.054268569
7.821707024	4.837130610	5.205374956
3.471966183	3.048284508	4.140193015
0.702532682	2.994390396	4.032689333
4.919146592	4.808572033	5.009930953
3.367855357	6.923629461	4.309898242
7.425199102	1.204959933	5.273722485
4.890307456	1.184844697	5.937431380
0.832650817	6.884124437	4.239464551
7.690565559	5.353940540	2.670350112
3.478461102	2.932723011	6.950612366
0.628612436	2.853760431	6.782123446
4.799618131	5.589694318	2.629219182
1.977447225	0.959821482	8.406034112
5.833428531	2.722384362	9.749953449
7.418193173	0.359396012	10.535782576
1.906997693	4.836350502	8.375999331
7.338010496	1.077632083	7.821602374
4.864542366	0.425669278	8.536157012
3.828846369	2.989002279	10.154230893
1.777155337	4.273544395	10.877092183
3.221985922	6.569488152	9.663318843
0.696449092	6.766576949	10.005072504
7.558381115	4.661087473	8.946709335
4.746301910	4.971878837	8.644141257
2.019463460	1.299490274	12.672339380
2.829639438	2.579040081	14.482830465
1.893035739	2.212149492	10.228955001
2.423808825	1.944630399	13.568073511

3.1.2 Al_2O_3-Co-CO_2 Configuration

The second model features a cobalt (Co) atom replacing the silver atom from the previous structure, while keeping the CO2 molecule in proximity. This model comprises of 63 atoms as well: 23 aluminum, 38 oxygen, 1 cobalt, and 1 carbon.

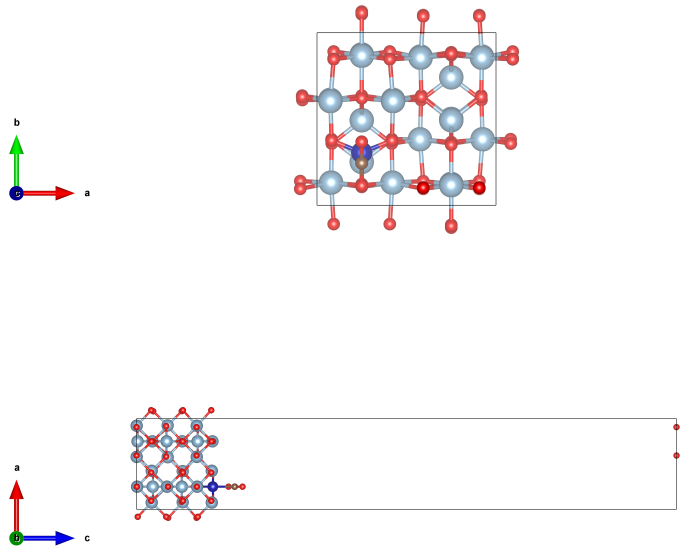

Figure 3.2: Top and side views of the Al_2O_3-Co-CO_2 relaxed structure.

Partial POSCAR content is given below:

```
Al2O3-Co-CO2 relaxed structure
1.0
        8.3723897934          0.0000000000          0.0000000000
        0.0000000000          8.0442800522          0.0000000000
        0.0000000000          0.0000000000         50.0000000000
   Al    O   Co    C
   23   38    1    1
Cartesian
     6.279292345          0.990653076          1.472219080
     2.093097448          6.998201955          2.825310268
```

2.093097448	3.966393217	4.199781269
6.279292345	4.022461755	0.097499823
6.279292345	0.960808843	4.239556193
2.093097448	7.028046008	0.057973200
6.279292345	5.965959631	2.796473540
2.093097448	2.022895101	1.500806771
0.627845484	4.912963647	1.410816237
4.814040194	3.075891324	2.886713110
7.744544496	3.075891324	2.886713110
3.558349350	4.912963647	1.410816237
4.843762618	6.934008688	0.018198375
0.657567472	1.054846403	4.279330745
3.528627425	1.054846403	4.279330745
7.714822072	6.934008688	0.018198375
6.279292345	0.935227995	7.033989578
6.279292345	3.967117226	5.659519136
2.093097448	6.972620927	5.619745329
0.627845484	4.857538566	6.972587854
3.558349350	4.857538566	6.972587854
4.843762618	6.878583607	5.579970032
7.714822072	6.878583607	5.579970032
6.279292345	7.002384908	4.273364693
2.093097448	0.986470064	0.023915624
2.093097448	5.114312113	2.778325975
6.279292345	2.874543098	1.519202441
6.279292345	7.131978283	1.385708340
2.093097448	0.856957180	2.911821194
2.093097448	5.043924490	0.110177498
6.279292345	2.944930482	4.187351838
3.404213677	7.167292683	4.297478497
7.590408574	0.821562348	0.000050900

4.968176116	0.821562348	0.000050900
0.781981219	7.167292683	4.297478497
7.689789063	4.909102423	2.747749723
3.503593917	3.079752548	1.549779531
0.682600917	3.079752548	1.549779531
4.868795627	4.909102423	2.747749723
3.405804346	6.863138232	1.361097489
7.591999492	1.125716499	2.936431952
4.966585198	1.125716499	2.936431952
0.780390426	6.863138232	1.361097489
7.681918809	5.112542365	0.112912024
3.495723912	2.876312846	4.184617475
0.690470985	2.876312846	4.184617475
4.876665881	5.112542365	0.112912024
2.093097448	0.931044983	5.585936457
6.279292345	2.819118018	7.080973685
6.279292345	7.076553203	6.947480142
2.093097448	4.988499409	5.671949312
7.590408574	0.766137207	5.561823025
4.968176116	0.766137207	5.561823025
3.503593917	3.024327467	7.111550868
0.682600917	3.024327467	7.111550868
3.405804346	6.807713152	6.922868639
0.780390426	6.807713152	6.922868639
7.681918809	5.057117284	5.674682930
4.876665881	5.057117284	5.674682930
2.093128887	0.911732510	8.519234508
2.091129760	2.961237476	9.819860756
2.093097448	2.459037673	7.062827051
2.090928275	1.967204630	9.093870223

3.1.3 [Al_2O_3-Cu-CO_2 Configuration]

The third model features a cobalt (Cu) atom replacing the silver atom from the previous structure, while keeping the CO2 molecule in proximity. This model comprises 63 atoms as well: 23 aluminum, 38 oxygen, 1 cobalt, and 1 carbon.

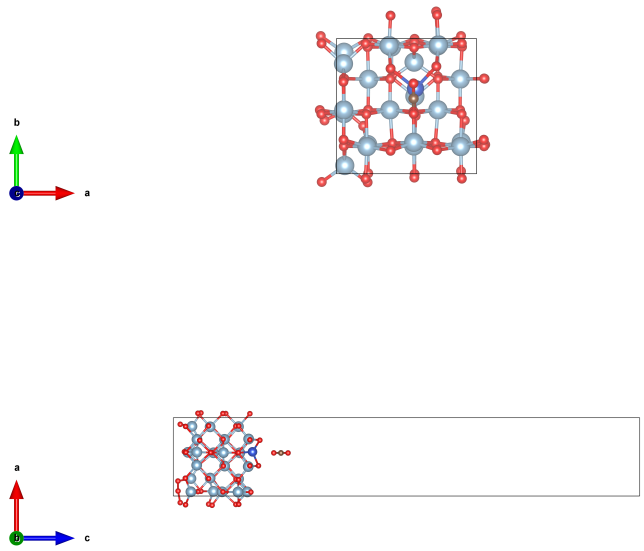

Figure 3.3: Al_2O_3-Cu-CO_2 structure visualized using VESTA..

POSCAR data (partial):

```
1.0
        8.3723897934          0.0000000000          0.0000000000
        0.0000000000          8.0442800522          0.0000000000
        0.0000000000          0.0000000000         50.0000000000
   Al    O   Cu    C
   22   39    1    1
Cartesian
     4.622529670           1.655282781           4.313287511
     4.638910439           6.646017868           5.378844962
```

0.454431624	7.231846516	1.890282147
0.451945565	3.584229385	5.230745673
4.671912011	1.774982759	1.567897573
0.501729378	0.492614829	4.311941192
4.687074141	4.614642027	2.533977292
3.291247006	7.548680722	2.510656230
7.395757134	5.635657411	3.949455172
1.920297929	5.624255940	3.951752186
6.052784116	7.615097321	2.539343759
7.452510198	1.872979475	2.006097324
3.201923784	3.802475560	5.505356565
6.060163321	3.804781842	5.487006903
1.870064736	1.735408930	1.898765750
0.442525656	3.801007882	7.935222983
0.424875284	6.548513934	6.937096268
4.617985473	1.876106501	7.137599587
3.145172218	7.627737759	8.033623546
6.096247922	7.669854971	8.079828322
7.415454479	1.617274442	6.995700300
1.826300637	1.614951379	7.008637488
0.443874481	1.638746716	5.627523363
4.732052513	3.445499825	1.195784472
4.652662799	7.816688402	4.004716873
0.473881666	5.658583098	2.643597312
0.511283745	1.735032781	2.966354229
4.640753868	3.590719818	4.171396047
4.668953243	8.030537778	1.343485806
0.445877850	5.671038937	5.322169885
5.906684626	1.841127015	5.681398511
0.535980000	3.753533720	0.513234269
7.666678830	3.172512782	0.747907022

3.339513009	1.827076198	5.669557303
1.864694888	7.536744156	3.794053197
6.049289385	5.788401828	2.621732838
3.290978775	5.742226327	2.620906755
7.500048611	7.556837575	3.792636842
5.955264022	1.612094179	2.835546434
1.896313889	3.803099838	4.191082343
7.386171702	3.790344326	4.162606969
3.352975930	1.620573840	2.785629220
1.902366664	0.027302860	1.291522756
6.069964835	5.637263657	5.347503349
3.211385456	5.638945181	5.366981030
7.440985522	0.153132613	1.317267306
4.610902693	3.707009400	6.873612106
0.419056462	5.474566747	8.320202678
0.428441220	2.025140489	8.213420212
4.636110862	7.509321459	6.976276636
1.783247910	3.543369121	6.731268764
7.476645445	3.555167118	6.710170209
5.967964420	6.391820069	9.281335771
3.235618514	6.255978636	9.132523090
6.010269970	1.404818785	8.209881932
3.234258149	1.367305386	8.204004169
1.739919716	7.753104070	6.995333731
7.488273421	7.755337471	7.020195574
4.610784921	3.578426042	10.776028037
4.603737073	5.377544207	12.303577363
1.602959398	2.852735790	0.501711061
4.724610429	5.070610711	8.494313061
4.606288631	4.479255617	11.543245614

3.1.4 INPUT FILE

Siesta SCF and Charge Density Calculation

```
 # Species and atoms
NumberOfAtoms      63
NumberOfSpecies       4
%block ChemicalSpeciesLabel
    1      13      Al
    2       8      O
    3      27      Co
    4       6      C
%endblock ChemicalSpeciesLabel

# Basis
PAO.BasisType         split
PAO.BasisSize         DZP

LatticeConstant  1.000000  Ang
%block LatticeVectors
    8.3723897934    0.0000000000    0.0000000000
    0.0000000000    8.0442800522    0.0000000000
    0.0000000000    0.0000000000   25.0000000000
%endblock LatticeVectors

AtomicCoordinatesFormat     Fractional
%block AtomicCoordinatesAndAtomicSpecies
    0.7500000000    0.1231499985    0.0588887632    1
    0.2500000000    0.8699600100    0.1130124107    1
    0.2500000000    0.4930700064    0.1679912508    1
    0.7500000000    0.5000399947    0.0038999927    1
```

0.7500000000	0.1194400042	0.1695822477	1
0.2500000000	0.8736699819	0.0023189278	1
0.7500000000	0.7416399718	0.1118589416	1
0.2500000000	0.2514699995	0.0600322708	1
0.0749899968	0.6107400060	0.0564326495	1
0.5749899745	0.3823699951	0.1154685244	1
0.9250100255	0.3823699951	0.1154685244	1
0.4250099957	0.6107400060	0.0564326495	1
0.5785400271	0.8619800210	0.0007279352	1
0.0785399973	0.1311299950	0.1711732298	1
0.4214600027	0.1311299950	0.1711732298	1
0.9214599729	0.8619800210	0.0007279352	1
0.7500000000	0.1162599995	0.2813595831	1
0.7500000000	0.4931600094	0.2263807654	1
0.2500000000	0.8667799830	0.2247898132	1
0.0749899968	0.6038500070	0.2789035142	1
0.4250099957	0.6038500070	0.2789035142	1
0.5785400271	0.8550900220	0.2231988013	1
0.9214599729	0.8550900220	0.2231988013	1
0.7500000000	0.8704800010	0.1709345877	2
0.2500000000	0.1226300001	0.0009566254	2
0.2500000000	0.6357700229	0.1111330390	2
0.7500000000	0.3573400080	0.0607680976	2
0.7500000000	0.8865900039	0.0554283336	2
0.2500000000	0.1065300032	0.1164728478	2
0.2500000000	0.6270200015	0.0044070999	2
0.7500000000	0.3660899997	0.1674940735	2
0.4065999984	0.8909800052	0.1718991399	2
0.9065999985	0.1021300033	0.0000020358	2
0.5934000015	0.1021300033	0.0000020358	2
0.0934000015	0.8909800052	0.1718991399	2

```
    0.9184700250    0.6102600097    0.1099099889    2
    0.4184699952    0.3828499913    0.0619911812    2
    0.0815299973    0.3828499913    0.0619911812    2
    0.5815299750    0.6102600097    0.1099099889    2
    0.4067899883    0.8531699776    0.0544438996    2
    0.9067900181    0.1399399936    0.1174572781    2
    0.5932099819    0.1399399936    0.1174572781    2
    0.0932099968    0.8531699776    0.0544438996    2
    0.9175300002    0.6355500221    0.0045164810    2
    0.4175300002    0.3575600088    0.1673846990    2
    0.0824699998    0.3575600088    0.1673846990    2
    0.5824699998    0.6355500221    0.0045164810    2
    0.2500000000    0.1157400012    0.2234374583    2
    0.7500000000    0.3504500092    0.2832389474    2
    0.7500000000    0.8797000051    0.2778992057    2
    0.2500000000    0.6201300025    0.2268779725    2
    0.9065999985    0.0952399969    0.2224729210    2
    0.5934000015    0.0952399969    0.2224729210    2
    0.4184699952    0.3759599924    0.2844620347    2
    0.0815299973    0.3759599924    0.2844620347    2
    0.4067899883    0.8462799788    0.2769147456    2
    0.0932099968    0.8462799788    0.2769147456    2
    0.9175300002    0.6286600232    0.2269873172    2
    0.5824699998    0.6286600232    0.2269873172    2
    0.2500037550    0.1133392304    0.3407693803    2
    0.2497649789    0.3681171537    0.3927944302    2
    0.2500000000    0.3056877256    0.2825130820    3
    0.2497409135    0.2445470095    0.3637548089    4
%endblock AtomicCoordinatesAndAtomicSpecies
 # Relaxation parameters
MD.TypeOfRun       CG
```

```
MD.NumCGsteps      100
MD.MaxForceTol     0.02 eV/Ang
MD.MaxStressTol    0.1 GPa
MD.VariableCell    false
#UseSaveData .true.
#MD.UseSaveXV .true.
#UseStructFile .true
# Electronic parameters
XC.functional      GGA
XC.authors         PBE
SolutionMethod     diagon
ElectronicTemperature  25 meV
DM.MixingWeight    0.1
DM.NumberPulay     5
DM.Tolerance       1e-4

# Output control
WriteDenchar       true
WriteCoorXmol      true
SaveRho            true
SaveElectrostaticPotential true
 # Relaxation parameters
MD.TypeOfRun       CG
MD.NumCGsteps      100
MD.MaxForceTol     0.02 eV/Ang
MD.MaxStressTol    0.1 GPa
MD.VariableCell    false

# Electronic parameters
XC.functional      GGA
XC.authors         PBE
```

```
SolutionMethod     diagon
ElectronicTemperature  25 meV
DM.MixingWeight    0.1
DM.NumberPulay     5
DM.Tolerance       1e-4

# Output control
WriteDenchar       true
WriteCoorXmol      true
SaveRho            true
SaveElectrostaticPotential true
# Output control
WriteDenchar       true
WriteCoorXmol      true
SaveRho            true
SaveElectrostaticPotential true
Denchar.TypeOfRun      3D

Denchar.PlotCharge          .true.
#Denchar.PlotWaveFunctions   .true.

Denchar.CoorUnits       Ang           # Format for coordinate of the points
                                       # Bohr
                                       # Ang

Denchar.DensityUnits   Ele/Ang**3     # Units of Charge Density
                                       # Ele/bohr**3
                                       # Ele/Ang**3
                                       # Ele/UnitCell

Denchar.MinX           00.0  Ang      # Minimum coord of the window in X-dir
```

```
Denchar.MaxX             9.0  Ang      # Maximum coord of the window in X-dir

Denchar.MinY            00.0  Ang      # Minimum coord of the window in Y-dir
Denchar.MaxY             9.0  Ang      # Maximum coord of the window in Y-dir

Denchar.MinZ            00.0  Ang      # Minimum coord of the window in Y-dir
Denchar.MaxZ             25.0  Ang      # Maximum coord of the window in Y-dir




Denchar.NumberPointsX    50             # Number of points in X-axis
Denchar.NumberPointsY    50             # Number of points in Y-axis
Denchar.NumberPointsZ    50             # Number of points in Y-axis

Denchar.PlaneGeneration  NormalVector      # Option to generate the plane
                                                 # NormalVector
                                                 # TwoLine
                                                 # ThreePoints
                                                 # ThreeAtomicIndices
Denchar.PlaneOrigin

Denchar.X-Axis
```

Computational Method

All calculations were carried out using the SIESTA (Spanish Initiative for Electronic Simulations with Thousands of Atoms) code, which is based on density functional theory (DFT). The exchange-correlation functional was treated within the generalized gradient approximation (GGA) using the Perdew-Burke-Ernzerhof (PBE) formulation. The self-consistent field (SCF) convergence was achieved using a Pulay-mixing scheme with a mixing weight of 0.1, five Pulay steps, and a density matrix tolerance of 10^{-4}. The electronic temperature was set to 25 meV to aid convergence.

Geometry optimization was performed using the conjugate gradient (CG) method with a maximum of 100 CG steps. Convergence criteria were set to a maximum force tolerance of 0.02 eV/Å and a maximum stress tolerance of 0.1 GPa. The cell size was kept fixed during relaxation (MD.VariableCell = false). The total energy was calculated using diagonalization of the Hamiltonian matrix (SolutionMethod = diagon).

To analyze charge distribution and potential fields, various outputs were enabled, including electron density, electrostatic potential, and charge density difference (CDD). Three-dimensional charge density maps were generated using the `Denchar` utility with a real-space grid of $50 \times 50 \times 50$ points over a region spanning 0–9 Å in the x and y directions and 0–25 Å in the z direction. The charge density was reported in units of electrons per $Å^3$, and visualization settings were chosen to allow effective analysis of adsorption and charge redistribution features.

3.2 Results and Discussion

3.2.1 Binding Energy Calculation

The binding energy (E_{bind}) of the CO_2 molecule on the Al_2O_3 + M system (where M = Co, Cu, Ag) is calculated using the following formula:

$$E_{\text{bind}} = E_{\text{Al}_2\text{O}_3+\text{M}+\text{CO}_2} - (E_{\text{Al}_2\text{O}_3+\text{M}} + E_{\text{CO}_2}) \tag{3.1}$$

where:

- $E_{\text{Al}_2\text{O}_3+\text{M}+\text{CO}_2}$ is the total energy of the combined system,
- $E_{\text{Al}_2\text{O}_3+\text{M}}$ is the energy of the substrate without CO_2,
- E_{CO_2} is the energy of the isolated CO_2 molecule.

A more negative binding energy indicates stronger adsorption of CO_2 on the surface.

Among the three investigated systems, the Al_2O_3 + Co + CO_2 structure exhibits the most negative binding energy, indicating a stronger interaction between the CO_2 molecule and the surface. This suggests that the Co-doped system is thermodynamically more stable compared to its Cu and Ag counterparts. The enhanced binding in the presence of Co may be attributed to its favorable electronic configuration and stronger affinity toward CO_2 adsorption.

3.3 Charge Density Difference Analysis

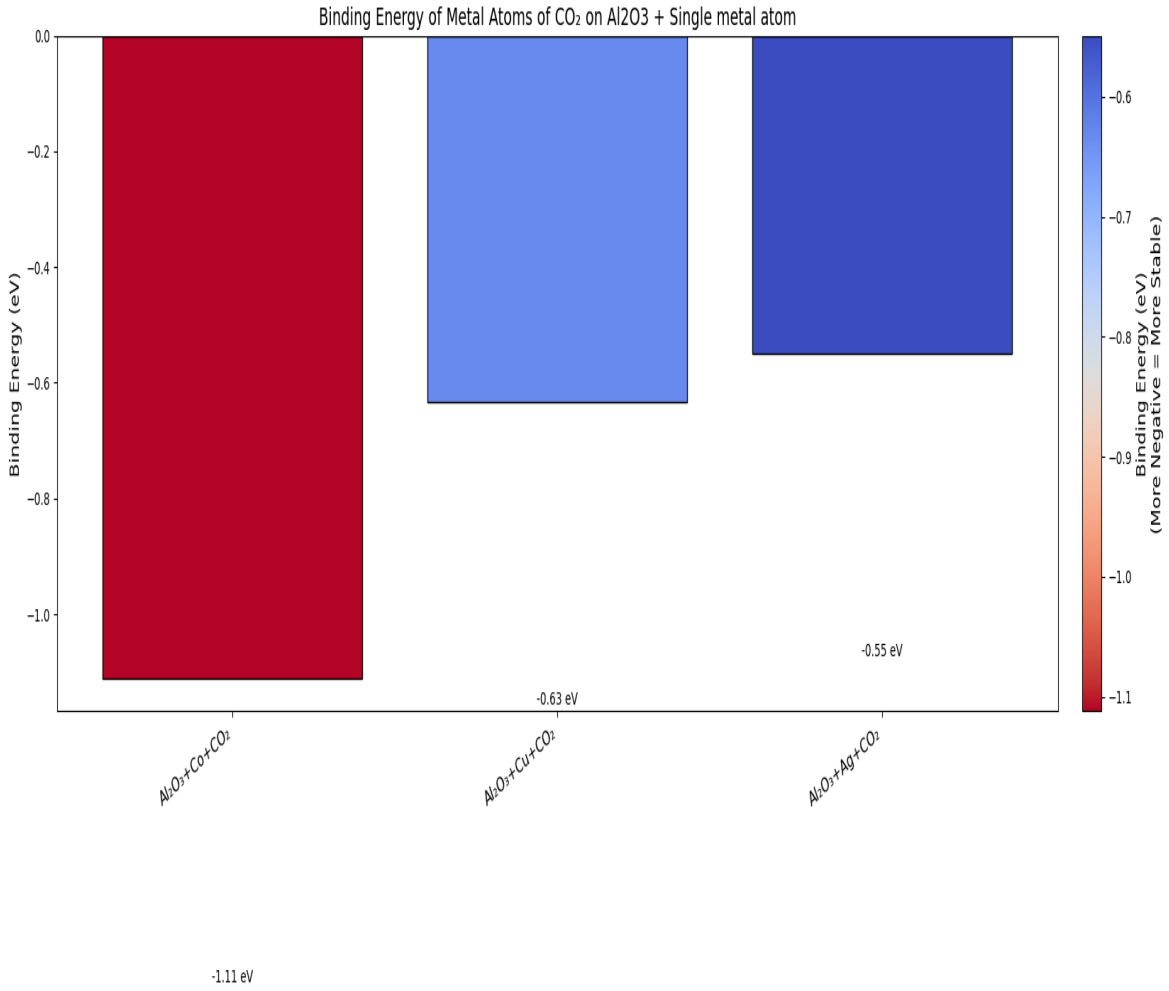

Figure 3.4: Binding energies of CO_2 on Al_2O_3 + M surfaces, where M = Co, Cu, and Ag.

3.3.1 Al_2O_3 + Co + CO_2 System

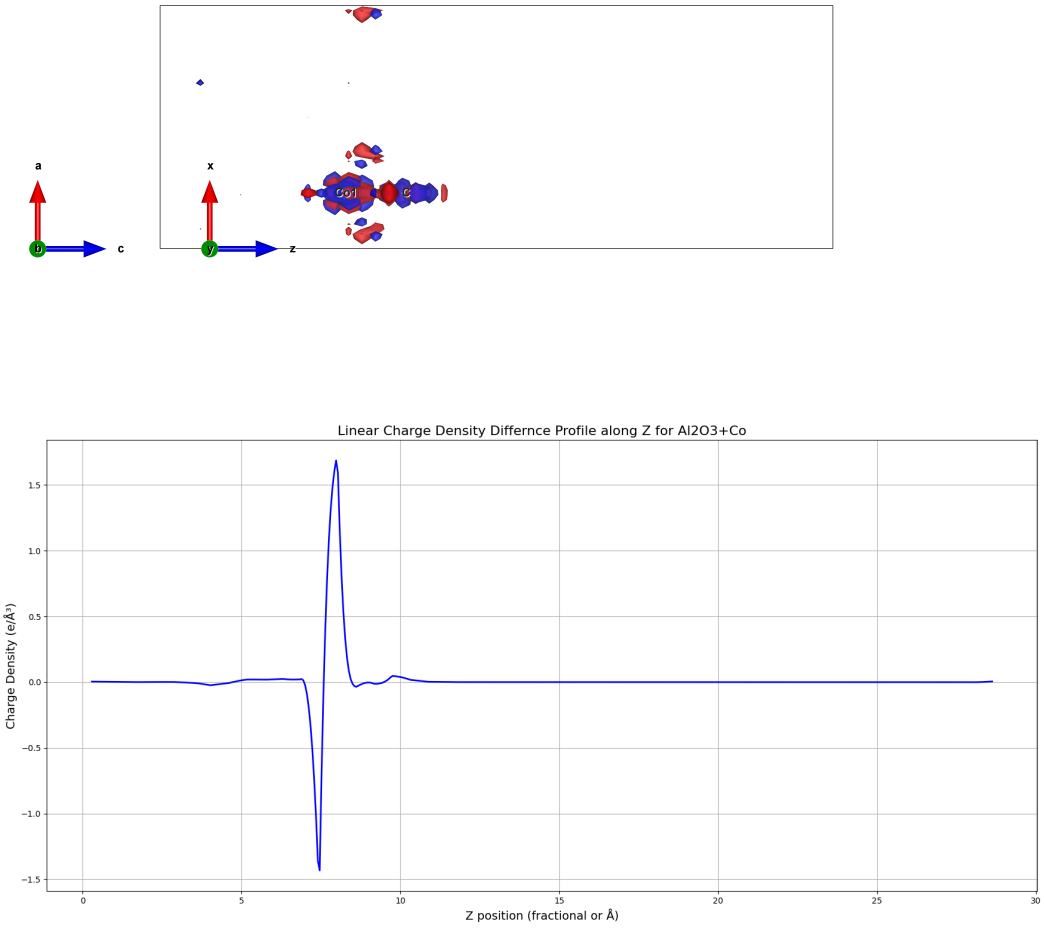

Figure 3.7: Charge density difference analysis for Al_2O_3 + Co + CO_2 system

3.3.2 Al_2O_3 + Cu + CO_2 System

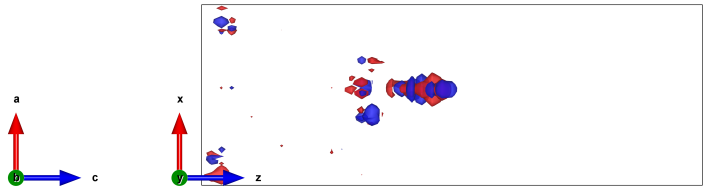

Figure 3.9: Charge density difference analysis for Al_2O_3 + Cu + CO_2 system

3.3.3 Al_2O_3 + Ag + CO_2 System

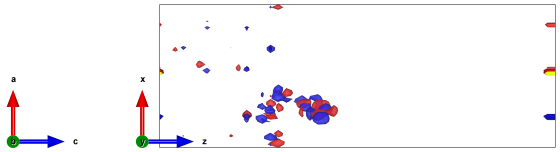

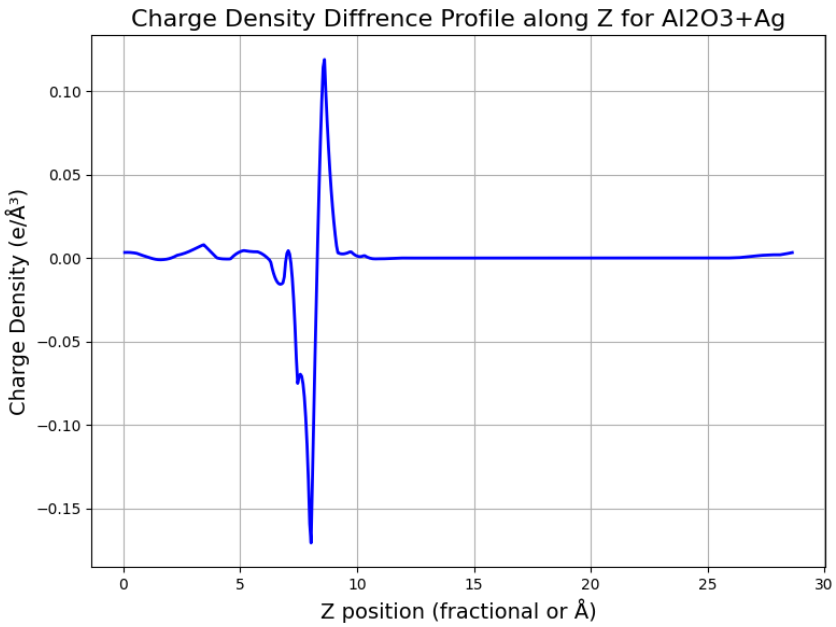

Figure 3.12: Charge density difference analysis for Al_2O_3 + Ag + CO_2 system

The planar-averaged charge density difference profiles along the z-direction for Al_2O_3 interfaced with Ag, Co, and Cu reveal distinct charge redistribution characteristics at the metal–oxide interface. Among the three, the Co/Al_2O_3 interface exhibits the most significant charge redistribution, with sharp and high-amplitude oscillations reaching up to ± 1.6 e/Å^3, indicating strong interfacial interaction and pronounced dipole formation. In contrast, the Ag/Al_2O_3 system shows moderate charge transfer, with symmetric peaks around ± 0.17 e/Å^3, suggesting a reasonably well-defined but weaker interface dipole. The Cu/Al_2O_3 interface, on the other hand, demonstrates the least charge rearrangement, with broad and shallow variations not exceeding ± 0.045 e/Å^3, indicating minimal bonding or interaction at the interface. Overall, the magnitude and spatial distribution of the charge density difference highlight that Co forms the strongest and most polarized interface with Al_2O_3, followed by Ag and then Cu.

3.3.4 Charge Density Difference Under Electric Field

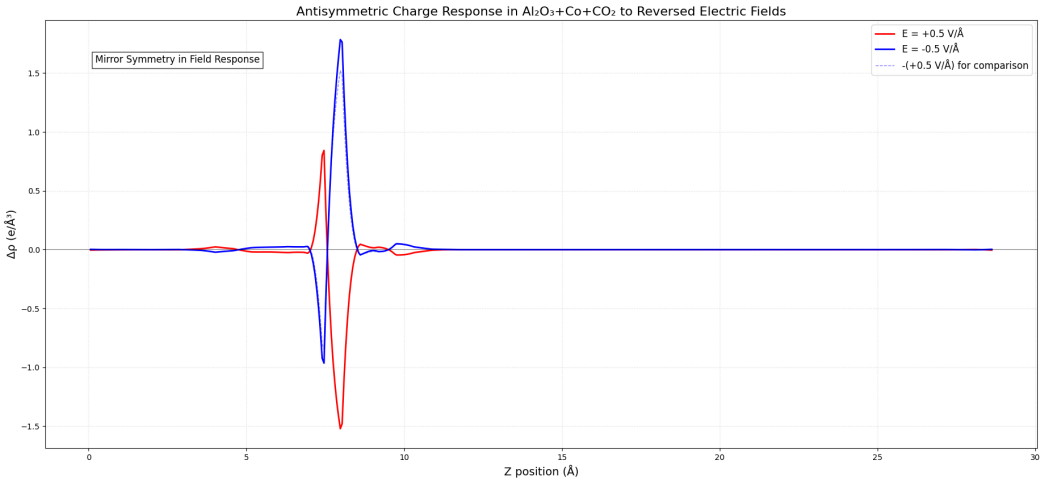
Antisymmetric Charge Response in Al₂O₃+Co+CO₂ to Reversed Electric Fields
Mirror Symmetry in Field Response
E = +0.5 V/Å
E = -0.5 V/Å
-(+0.5 V/Å) for comparison
Δρ (e/Å³)
Z position (Å)

Figure 3.13: Linear profile of charge density difference (CDD) along Z-axis for Al_2O_3 + Co + CO_2 system under applied electric fields (E = +0.5 V/Å, red curve and E = -0.5 V/Å, blue curve)

Figure 3.13 illustrates the antisymmetric planar-averaged charge density difference ($\Delta\rho$) along the z-axis for the Al_2O_3+Co+CO_2 heterostructure subjected to reversed

external electric fields of $+0.5$ V/Å and -0.5 V/Å. The red and blue curves represent the field-induced charge redistributions under positive and negative electric fields, respectively, while the dashed blue line depicts the inverted profile of the $+0.5$ V/Å case for comparison. A near-perfect mirror symmetry is observed between the responses to opposite field directions, emphasizing the linear and antisymmetric behavior of the system's charge response. This symmetry strongly suggests that the charge redistribution is predominantly field-driven and reversible, with no notable asymmetry or hysteresis effects. The pronounced peak and dip around the interface region indicate substantial polarization localized at the metal–oxide junction, with minimal charge response further away from the interface.

SUMMARY AND CONCLUSION

Chapter 4

SUMMARY AND CONCLUSION

Summary

In this thesis, we investigated the interaction of CO_2 molecules with Al_2O_3 surfaces modified by transition metals (M = Cu, Co, Ag) using density functional theory (DFT) calculations within the SIESTA framework. The study focused on evaluating the binding energy of CO_2 on each doped surface and analyzing the corresponding charge redistribution using charge density difference (CDD) plots, particularly under reversed electric fields.

Our calculations revealed that the Al_2O_3 + Co + CO_2 system exhibits the most negative binding energy among the three, indicating a significantly stronger interaction between the CO_2 molecule and the Co-doped surface. This suggests that Co offers a more stable and energetically favorable site for CO_2 adsorption, likely due to its electronic configuration and higher chemical reactivity. In comparison, the Cu- and Ag-doped systems show weaker adsorption characteristics. Additionally, the CDD analysis revealed a nearly symmetric charge response to reversed electric fields, especially in the Co system, indicating a strong, linear polarization behavior.

Conclusion

The findings of this study highlight the superior adsorption and electronic response characteristics of the Al_2O_3 + Co + CO_2 system, making it the most promising candidate among the investigated configurations. The strong binding energy and antisymmetric charge redistribution in the presence of electric fields suggest that Co doping enhances the chemical and electrostatic interaction with CO_2, potentially offering advantages in applications such as gas sensing, catalysis, and field-effect control of adsorption.

These results provide valuable insight into the role of transition metal dopants in tuning surface reactivity and responsiveness to external stimuli. Future work can expand on this foundation by examining temperature-dependent behavior, exploring spin polarization effects, or integrating dynamic field applications to further assess the viability of these systems in practical energy and sensing technologies.

References

[1] M. Kampa and E. Castanas. "Human health effects of air pollution". In: *Environmental Pollution* 151 (2008), pp. 362–367.

[2] A.C. Stern. *Fundamentals of Air Pollution*. Elsevier, 2014.

[3] J.F. Mitchell. "The "greenhouse" effect and climate change". In: *Reviews of Geophysics* 27.1 (1989), pp. 115–139.

[4] D.A. Lashof and D.R. Ahuja. "Relative contributions of greenhouse gas emissions to global warming". In: *Nature* 344 (1990), pp. 529–531.

[5] B. Liu and B. Smit. "Molecular simulation studies of separation of CO_2/N_2, CO_2/CH, and CH/N_2 by ZIFs". In: *The Journal of Physical Chemistry C* 114 (2010), pp. 8515–8522.

[6] H. et al. Furukawa. "Ultrahigh porosity in metal-organic frameworks". In: *Science* 329 (2010), pp. 424–428.

[7] G. et al. Férey. "Why hybrid porous solids capture greenhouse gases?" In: *Chemical Society Reviews* 40 (2011), pp. 550–562.

[8] Q. et al. Wang. "CO_2 capture by solid adsorbents and their applications: current status and new trends". In: *Energy Environmental Science* 4 (2011), pp. 42–55.

[9] H. et al. Guo. "CO_2 capture on h-BN sheet with high selectivity controlled by external electric field". In: *The Journal of Physical Chemistry C* 119 (2015), pp. 6912–6917.

[10] T.C. et al. Drage. "Evaluation of activated carbon adsorbents for CO_2 capture in gasification". In: *Energy Fuels* 23 (2009), pp. 2790–2796.

[11] M.G. et al. Plaza. "Post-combustion CO_2 capture with a commercial activated carbon: comparison of different regeneration strategies". In: *Chemical Engineering Journal* 163 (2010), pp. 41–47.

[12] M. et al. Cinke. "CO_2 adsorption in single-walled carbon nanotubes". In: *Chemical Physics Letters* 376 (2003), pp. 761–766.

[13] F. et al. Su. "Capture of CO_2 from flue gas via multiwalled carbon nanotubes". In: *Science of The Total Environment* 407 (2009), pp. 3017–3023.

[14] T.M. et al. McDonald. "Cooperative insertion of CO_2 in diamine-appended metal-organic frameworks". In: *Nature* 519 (2015), p. 303.

[15] J.C. et al. Abanades. "Emerging CO_2 capture systems". In: *International Journal of Greenhouse Gas Control* 40 (2015), pp. 126–166.

[16] Y. et al. Zeng. "Covalent organic frameworks for CO_2 capture". In: *Advanced Materials* 28 (2016), pp. 2855–2873.

[17] B. Qiao et al. "Single-atom catalysis of CO oxidation using Pt1/FeOx". In: *Nature Chemistry* 3 (2011), pp. 634–641.

[18] J. Liu. "Catalysis by supported single metal atoms". In: *ACS Catalysis* 7 (2019), pp. 34–59.

[19] H. Yamashita, M. Tada, and K. Kaneda. "Design of SACs on reducible oxide supports for selective CO_2 conversion". In: *Chemical Society Reviews* 50 (2021), pp. 1893–1912.

[20] Q. Zhai, G. Sun, and J. Sun. "Role of oxygen vacancies in CO_2 adsorption and activation on CeO_2". In: *Applied Catalysis B: Environmental* 272 (2020), p. 119026.

[21] X. Li, X. Yang, and Y. Huang. "Stabilization of single atoms on irreducible oxide supports for CO_2 reduction". In: *Nature Communications* 12 (2021), p. 1231.

[22] Y. He, Z. Lin, and Y. Zhu. "Electric field enhanced CO_2 activation on single-atom catalysts". In: *ACS Applied Materials & Interfaces* 12 (2020), pp. 18948–18956.

[23] Y. Wang, Y. Zhao, and W. Chen. "Electric field modulation of CO_2 reduction on SACs: A DFT study". In: *Journal of Materials Chemistry A* 6 (2018), pp. 22063–22071.

[24] Klaus Kähler, Tina Franzke, and Martin Muhler. "Thermochemical CO_2 Activation". In: *Chemical Energy Storage*. De Gruyter, 2013, pp. 401–419. DOI: 10.1515/9783110266320.401.

[25] H. Zhang et al. "Impacts of the Catalyst Structures on CO_2 Activation on Catalyst Surfaces". In: *Materials* 11.12 (2022), p. 3265. URL: https://www.mdpi.com/2079-4991/11/12/3265.

[26] F. Doherty and B. R. Goldsmith. "Modeling plasma-induced surface charge effects on CO_2 activation by single atom catalysts supported on reducible and irreducible metal oxides". In: *Plasma Sources Science and Technology* 32.3 (2023), p. 035008. DOI: 10.1088/1361-6595/acc19f.

[27] Brian Harold Bransden and Charles Jean Joachain. *Physics of atoms and molecules*. Pearson Education India, 2003.

[28] Pierre Hohenberg and Walter Kohn. "Inhomogeneous electron gas". In: *Physical review* 136.3B (1964), B864.

[29] Walter Kohn and Lu Jeu Sham. "Self-consistent equations including exchange and correlation effects". In: *Physical review* 140.4A (1965), A1133.

prashik

ORIGINALITY REPORT

24%	21%	16%	%
SIMILARITY INDEX	INTERNET SOURCES	PUBLICATIONS	STUDENT PAPERS

PRIMARY SOURCES

1	www.repository.cam.ac.uk Internet Source	4%
2	www.scribd.com Internet Source	3%
3	www.mail-archive.com Internet Source	2%
4	www.coursehero.com Internet Source	1%
5	vnit.ac.in Internet Source	1%
6	vdocuments.mx Internet Source	1%
7	fys.kuleuven.be Internet Source	1%
8	ikee.lib.auth.gr Internet Source	1%
9	doczz.net Internet Source	1%
10	Ferdous, Naim. "Two-Dimensional van der Waals Bilayer Heterostructure Towards Band-to-Band Tunneling and Photocatalytic Water Splitting Applications.", University of Nevada, Reno Publication	<1%
11	moam.info	

	Internet Source	<1%
12	documents.mx Internet Source	<1%
13	mzuir.inflibnet.ac.in Internet Source	<1%
14	Denis Misiurev, Vladimír Holcman. "Modeling of Magnetic Films: A Scientific Perspective", Materials, 2024 Publication	<1%
15	purehost.bath.ac.uk Internet Source	<1%
16	ruor.uottawa.ca Internet Source	<1%
17	dspace.alquds.edu Internet Source	<1%
18	Barker, Bradford Alan. "Electronic and Optical Properties of Solids with Strong Spin-Orbit Coupling.", University of California, Berkeley, 2018 Publication	<1%
19	repository.kaust.edu.sa Internet Source	<1%
20	www.dspace.cam.ac.uk Internet Source	<1%
21	Guo, Qing. "Application of Graphene-Based 2d Materials and Exploration of Lithium Polysulfides Solid Phases – First-Principles Study Based on Density Functional Theory", Michigan Technological University, 2021 Publication	<1%

22	Mohammad, Rezek. "The Electronic Band Structure of iii (IN, AL, GA)-v (N, AS, SB) Compounds and Ternary Alloys", Middle East Technical University (Turkey), 2024 Publication	<1 %
23	kobra.uni-kassel.de Internet Source	<1 %
24	Francis Doherty, Bryan Goldsmith. " Modeling plasma-induced surface charge effects on CO activation by single atom catalysts supported on reducible and irreducible metal oxides ", Plasma Sources Science and Technology, 2023 Publication	<1 %
25	"Handbook of Materials Modeling", Springer Science and Business Media LLC, 2005 Publication	<1 %
26	dx.doi.org Internet Source	<1 %
27	materials-sciences-algerien1970.blogspot.com Internet Source	<1 %
28	pdffox.com Internet Source	<1 %
29	udspace.udel.edu Internet Source	<1 %
30	Jenő Sólyom. "Cohesive Energy of the Electron System", Fundamentals of the Physics of Solids, 2010 Publication	<1 %
31	Lin Yuan, Qinglong Fang, Baiyu Zhang. "Theoretical exploration of the nitrogen	<1 %

	fixation mechanism of two-dimensional dual-metal FeTM@GY (TM = Fe, Mo, Co, and V) electrocatalysts", Dalton Transactions, 2024 Publication	
32	gyan.iitg.ernet.in Internet Source	<1 %
33	hdl.handle.net Internet Source	<1 %
34	pubs.rsc.org Internet Source	<1 %
35	uu.diva-portal.org Internet Source	<1 %
36	www.researchgate.net Internet Source	<1 %
37	Zhu, Hao. "Materials design and synthesis for desirable magnetic and optical properties", Proquest, 20111004 Publication	<1 %
38	fse.studenttheses.ub.rug.nl Internet Source	<1 %
39	www.mdpi.com Internet Source	<1 %
40	Huashuo Zhang, Maohuai Wang, Shoufu Cao, Zengxuan Chen et al. "N, S coordination in Co single atom catalyst promoting CO2RR towards HCOOH at negative potentials", Molecular Catalysis, 2025 Publication	<1 %
41	L. M. Sandratskii. "Noncollinear magnetism in itinerant-electron systems: Theory and applications", Advances in Physics, 1998 Publication	<1 %

42	orca.cf.ac.uk Internet Source	<1 %
43	ethesis.nitrkl.ac.in Internet Source	<1 %
44	publikationen.ub.uni-frankfurt.de Internet Source	<1 %
45	wiredspace.wits.ac.za Internet Source	<1 %
46	www.fzu.cz Internet Source	<1 %
47	Tetsuya Morishita, Salvy P. Russo, Ian K. Snook, Michelle J. S. Spencer, Kengo Nishio, Masuhiro Mikami. "First-principles study of structural and electronic properties of ultrathin silicon nanosheets", Physical Review B, 2010 Publication	<1 %
48	etd.aau.edu.et Internet Source	<1 %
49	1library.org Internet Source	<1 %
50	Senozan, Selma. "First-Principles Study of GaAs/AlAs Nanowire Heterostructures.", Middle East Technical University (Turkey), 2024 Publication	<1 %
51	Xiong, Chuanye. "Novel Single-Atom Catalysts (SACs) Design Based on First Principles", University of California, Riverside, 2024 Publication	<1 %
52	etheses.whiterose.ac.uk Internet Source	<1 %

53	Qi, Ji. "Insights Into Solid Electrolytes From Long-Time and Large-Size Scale Simulations With Machine Learning Interatomic Potentials", University of California, San Diego, 2024 Publication	<1 %
54	dr.ntu.edu.sg Internet Source	<1 %
55	era.library.ualberta.ca Internet Source	<1 %
56	studylib.net Internet Source	<1 %
57	www.technicaltextile.net Internet Source	<1 %
58	Haihong Huang, Zhengchun Qian, Zhifeng Liu. "Metal Magnetic Memory Technique and Its Applications in Remanufacturing", Springer Science and Business Media LLC, 2021 Publication	<1 %
59	Price, Conor Jason. "Ab Initio Study of Intercalated TMDCs and Their Superlattices", University of Exeter (United Kingdom), 2024 Publication	<1 %
60	chemistry-europe.onlinelibrary.wiley.com Internet Source	<1 %
61	docplayer.net Internet Source	<1 %
62	etda.libraries.psu.edu Internet Source	<1 %
63	fdocuments.us Internet Source	<1 %

64	ijsret.com Internet Source	<1 %
65	3e4df83c-8e29-463e-b655-c175ccee6d8c.filesusr.com Internet Source	<1 %
66	Sharma, Shivam. "Exploitation of Symmetries of Quantum Mechanics in Nanostructures", University of Minnesota, 2025 Publication	<1 %
67	www.adroitmarketresearch.com Internet Source	<1 %
68	Nilkamal, Som Narayan. "Tailoring Electronic, Machanical and Dynamical Properties of Two Dimensional Materials Using Density Functional Theory", Maharaja Sayajirao University of Baroda (India), 2020 Publication	<1 %
69	ir.library.osaka-u.ac.jp Internet Source	<1 %
70	repository.upenn.edu Internet Source	<1 %
71	www.escholar.manchester.ac.uk Internet Source	<1 %
72	www.euromof2023.com Internet Source	<1 %
73	www.solubilityofthings.com Internet Source	<1 %
74	Bohuslav Dobias, Hansjoachim Stechemesser. "Coagulation and Flocculation", CRC Press, 2019 Publication	<1 %

75	Zhang, Buyu. "Machine Learning Potentials and Investigation of Interstitials in Metals", University of California, Berkeley Publication	<1 %
76	pdxscholar.library.pdx.edu Internet Source	<1 %
77	Electronic Density Functional Theory, 1998. Publication	<1 %
78	Rajendra Prasad. "Electronic Structure of Materials", CRC Press, 2019 Publication	<1 %
79	Teixeira, Sofia Ferreira. "Bi-Te and Sb-Te Topological Insulator Materials: From First Principle Calculations Towards Nanostructures Fabrication", Universidade do Porto (Portugal), 2024 Publication	<1 %
80	Vassaux, Antoine. "Mécanisme de Biosynthèse et Production de L'astine, un Pentapeptide Cyclique Non-Ribosomique de Cyanodermella Asteris", Universite de Liege (Belgium), 2024 Publication	<1 %
81	Yildirim, Handan. "Structural, electronic, vibrational and thermodynamical properties of surfaces and nanoparticles", Proquest, 20111108 Publication	<1 %

Exclude quotes	Off	Exclude matches	Off
Exclude bibliography	On		